Probing Interactions between Electron Donors and the Support in MgCl₂-Supported Ziegler−Natta Catalysts

E. S. Merijn Blaakmeer,[†,‡] Giuseppe Antinucci,[‡,§] Ernst R. H. van Eck,[†] and Arno P. M. Kentgens[†,*]

†Radboud University, Institute for Molecules and Materials, Heyendaalseweg 135, 6525 AJ Nijmegen, The Netherlands
‡Dutch Polymer Institute (DPI), P.O. Box 902, 5600 AX Eindhoven, The Netherlands
§Laboratory of Stereoselective Polymerizations, Federico II University of Naples, Via Cintia, 80126 Naples, Italy

Ⓢ *Supporting Information*

ABSTRACT: Olefin polymerization using Ziegler−Natta catalysts (ZNCs) is an important industrial process. Despite this, fundamental insight into the inner working mechanisms of these catalysts remains scarce. Here, we focus on the low-γ nuclei ^{25}Mg and ^{35}Cl for an in-depth solid-state NMR and density functional theory (DFT) study of the catalyst's MgCl₂ support in binary adducts prepared by ball-milling. Besides the bare MgCl₂ support and a MgCl₂−TiCl₄ adduct, samples containing donors that are part of the families of 2,2-dialkyl-1,3-dimethoxypropanes and phthalates used in fourth- and fifth-generation ZNCs are studied. DFT calculations indicate that the quadrupolar coupling parameters of the chlorines differ significantly between bulk and surface sites. As a result, the NMR visibility of the chlorine sites correlates with the particle size except for the adduct with 2,2-dimethyl-1,3-dimethoxypropane donor. The DFT calculations furthermore show that the surface sites are fairly insensitive to binding of different donor molecules, making it difficult to identify specific binding motives. The surface sites with large ^{35}Cl NMR line widths can be observed using high radio frequency field strengths. For the 2,2-dimethyl-1,3-dimethoxypropane donor, we observe additional surface sites with intermediately high quadrupolar couplings, suggesting a different surface structure for this particular adduct compared to the other systems. For ^{25}Mg, pronounced effects of donor binding on the quadrupole interaction parameters are observed, both computationally and experimentally. Again the adduct with the 2,2-dimethyl-1,3-dimethoxypropane donor shows a different behavior of the surface sites compared to the other adducts, which display more asymmetric coordinations of the surface Mg sites. Identifying specific binding motives by comparing ^{25}Mg NMR results to DFT calculations also proves to be difficult, however. This is attributed to the existence of many defect structures caused by the ball-milling process. The existence of such defect structures both at the surface and in the interior of the MgCl₂ particles is corroborated by NMR relaxation studies. Finally, we performed heteronuclear correlation experiments, which reveal interactions between the support and Mg−OH surface groups, but do not provide indications for donor−surface interactions.
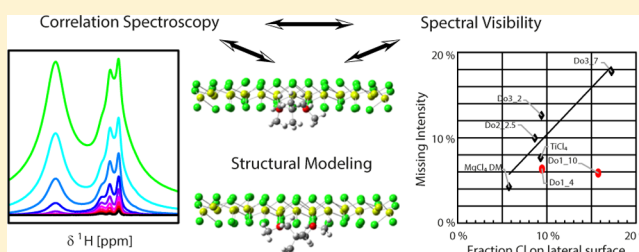
INTRODUCTION

Ziegler−Natta catalysts (ZNCs) play an important role in the worldwide production of polyolefins. Modern catalysts are composed of a disordered MgCl₂ support with co-adsorbed TiCl₄ and an organic electron donor. This system is activated by an Al-alkyl, often together with a second donor (in most cases, an alkoxysilane).[1,2] Still, these catalysts hold many secrets at the molecular level. The important surface structures are not well understood, due to the complexity of the system and the absence of significant experimental studies. Yet, fundamental understanding of the active constructs is crucial for further catalyst design.

The last decade yielded a significant number of theoretical contributions aimed at finding the most stable surface constructs for MgCl₂−donor or MgCl₂−TiCl₄ binary adducts.[3−16] Thermodynamically, (104)-surface sites have been found to be the most stable. However, coordination of electron donors can reverse the relative stabilities so that the (110)-surface sites become more stable than the (104)-surface.[5,7,14,17,18] Some computational studies go one step further and look at the role that the donors play in the whole catalytic cycle.[19−21]

Recent years have seen more experimental studies that focus on structure−function relationships, for both traditional MgCl₂-based ZNCs[22−24] and new MgCl₂-derived support materials.[25−29] Still, many studies try to investigate the produced polymer in intricate ways to learn more about these elusive catalysts via an indirect approach.[30] It is our belief that the final answers about the working mechanisms of ZNCs will primarily be found when studying the catalysts themselves.[31]

Table 1. Sample Properties

samples code	donor loading[a]	$\langle L_c \rangle$ (nm)	$\langle L_a \rangle$ (nm)	Cl surf. frac.[b] (%) (104)/(110)	rel. int.[c] (%)	Mg surf. frac.[b] (%) (104)/(110)
dry MgCl$_2$[d]		n.d.[e]	n.d.[e]		100	
MgCl$_2$ DCM[d]		12.6	13.0	**5.3**[f]/6.2	96	**10.5**/6.2
MgCl$_2$/TiCl$_4$	4.3	6.34	7.88	8.4/**10.2**	92	16.8/**10.0**
Do1_4	4.0	4.24	7.70	8.6/**10.3**	94	17.0/**10.0**
Do1_10	10.0	2.84	4.37	14.3/**17.2**	93	28.3/**17.0**
Do2_2.5	2.5	4.98	8.41	8.0/**9.3**	91	15.8/**9.5**
Do3_2	2.1	7.35	7.76	**8.5**/10.3	87	**16.9**/10.0
Do3_7	6.7	n.d.[e]	3.93	**15**/19	82	**31.0**/19.5

[a](% mol adsorbate/mol mg). [b]The fraction of surface sites is given for particles exposing either (104)- or (110)-surface sites, see text. [c]35Cl intensities from solid-state NMR experiments are an average between magic-angle spinning (*MAS*) and static relative intensities, where the difference between MAS and static was never more than 3%. [d]See ref 42. [e]The average size could not be determined because the XRD resonances were too narrow (dry MgCl$_2$) or too broad (Do3_7). [f]Numbers in bold face indicate most probable exposed surface.

This calls for a wide range of experimental studies making use of the strengths of different spectroscopic techniques, including solid-state NMR spectroscopy. A few recent studies[32−34] have shown the potential of a combined ^{1}H and ^{13}C solid-state NMR/density functional theory (DFT) approach for the study of the organic donors on the catalysts' surface, giving valuable experimental proof for standing hypothesis about preferred coordination modes. The surface structures in Ziegler−Natta catalysts can be studied from two sides. Besides the donor, the support can be studied. One of the strengths of NMR spectroscopy is its ability to study interactions between different components, such as donor−support interactions, making it a suitable tool for the study of heterogeneous catalysis.[35,36] Such insight into donor−support interactions should give a more complete picture of the coordination of donors on the MgCl$_2$−support. In this article, we will present a detailed investigation of the MgCl$_2$ nanoparticles' surface. Subsequently, we will present an in-depth study of the interactions between the donors and the surface. To this end, we make use of correlation experiments, such as cross-polarization (CP), rotational-echo double-resonance (REDOR),[37,38] and transfer of populations in double resonance (TRAPDOR).[39−41]

In a previous study, we showed the feasibility of [25]Mg and [35]Cl solid-state NMR for the study of the neat support material MgCl$_2$ (α-MgCl$_2$) as well as the ball-milled equivalent (δ-MgCl$_2$).[42] The results indicated that the bulk of MgCl$_2$ nanoparticles is readily observed; however, more advanced schemes are necessary to study the catalytic relevant surfaces because of their large quadrupolar interactions. Here, we will use ^{1}H, [25]Mg, and [35]Cl solid-state NMR to study the support with its surfaces and support−donor interactions in Ziegler−Natta catalyst model systems. We will make use of a variety of sensitivity enhancement schemes and correlation experiments to yield information about the surface structures. The interpretation of the NMR results is supported by DFT calculations of both [25]Mg and [35]Cl quadrupolar interaction parameters.

■ RESULTS AND DISCUSSION

A series of ball-milled binary adducts between MgCl$_2$ and industry-relevant electron donors and an adduct between MgCl$_2$ and TiCl$_4$ are studied. The investigated samples have been introduced by us elsewhere[34] and studied with ^{13}C NMR spectroscopy to identify the preferences for particular surfaces depending on the donor type. The samples contain donors that are part of the families of 2,2-dialkyl-1,3-dimethoxypropanes

and phthalates: 2,2-dimethyl-1,3-dimethoxypropane (DMDOMe, Do1), 9,9-bis(methoxymethyl)-9*H*-fluorene (DMFluo, Do2), and diisobutyl phthalate (DiBP, Do3) used in fourth- and fifth-generation ZNCs.[43,44] The binary adducts are coded as Do"*x*"_"*y*", where Do"*x*" refers to the donor type and _"*y*" refers to the donor loading (in percentage). Table 1 gives the sample characteristics showing the particle size as determined from powder X-ray diffraction (XRD), where $\langle L_c \rangle$ and $\langle L_a \rangle$ are the average particle dimensions perpendicular and parallel to the basal (*ab*) plane, respectively. Ball milling MgCl$_2$ in the presence of electron donors yields nanoparticles with much smaller dimensions. On the basis of previous results,[34] we printed the most likely surface type for each sample in bold.

The MgCl$_2$ nanoparticles can be studied by [25]Mg and [35]Cl NMR. We compare the binary adducts to neat MgCl$_2$ as well as the ball-milled equivalent (MgCl$_2$ DCM) for quantitative measurements of the [35]Cl NMR signal intensity. Despite large surface areas, these particles still have a dominant "bulk" phase, which will be the predominant species in [25]Mg and [35]Cl spectra. Therefore, we will first characterize the bulk phase in detail before performing dedicated NMR experiments that are necessary to look at the surfaces. With the surface sites revealed, correlation experiments can be performed to probe interactions between donor and support.

In studies of Ziegler−Natta catalysts, there are two types of surfaces of the MgCl$_2$ nanoparticles that are most commonly considered: the (104)- and (110)-surfaces. The (104)-surface is supposedly the most stable lateral surface of MgCl$_2$ in the absence of donors. It exposes pentacoordinated magnesium sites as well as coordinatively unsaturated chloride sites that are bound to only two magnesium. On this surface, donors might bind monodentately, although bivalent donors are more inclined to bind in a bridging mode. In the presence of electron donors, also the (110)-type of surfaces might become exposed because of the stabilizing effect of the donor. The (110)-surface exposes tetracoordinated magnesium sites on which bivalent donors coordinate in a chelating mode. Again, there are coordinatively unsaturated chloride sites as well.

Ball milling MgCl$_2$ yields nanoparticles with the high surface areas needed for catalysis. The fraction of surface sites/exposed sites (also called "surface fraction" in short) is defined as the number of coordinatively unsaturated Mg or Cl atoms (the outermost layer) divided by the total number of Mg or Cl sites in the nanoparticles. An estimation of this fraction of surface sites can be made for particular particle geometries from the given $\langle L_c \rangle$ and $\langle L_a \rangle$ dimensions, and the results are shown in Table 1 for hexagonal particles exposing either (104)- or
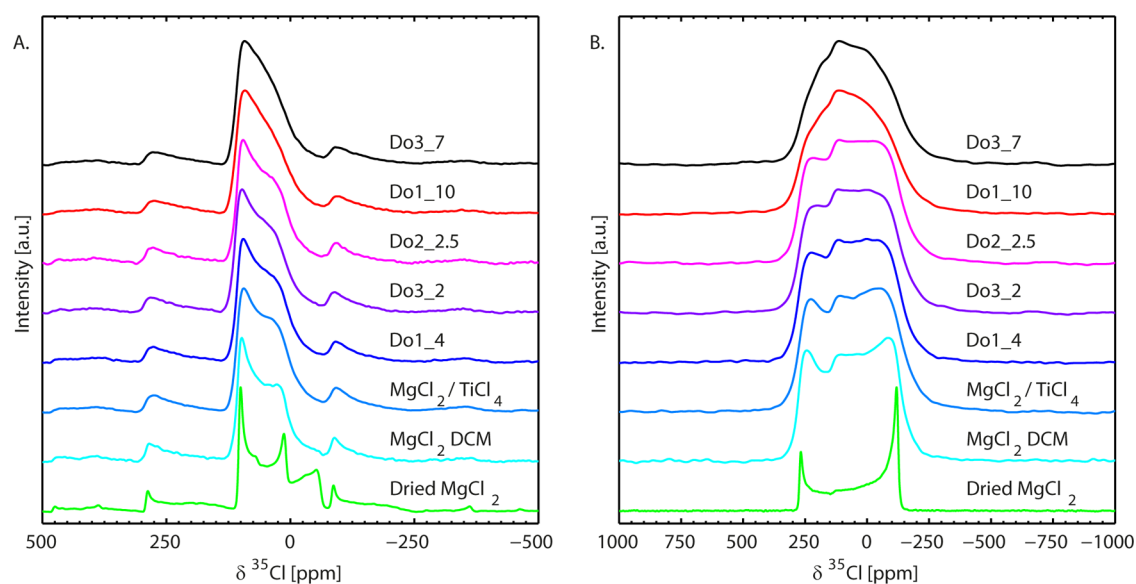
Figure 1. ^{35}Cl NMR Hahn-echo spectra of MgCl$_2$ binary adducts (A) at 15.625 kHz MAS, rotor-synchronized and (B) under static conditions, B_0 = 20 T.

(110)-type surfaces. Figure S1 shows the crystallographic morphology of such a hexagonal particle.

For chlorine, particles with only (110)-type surface sites yield a 20−30% higher fraction of surface sites than equisized particles with only (104)-type surfaces, depending on the exact particle size (see Table 1). For example, with a particle size of 13 nm, the ball-milled sample has an estimated chlorine surface fraction of 5.3% (considering only (104)-surfaces) or 6.2% (assuming only (110)-surfaces), so the adduct with the smallest particle size (Do3_7) has a surface fraction of 15−19.5%. The difference in the fraction of exposed surface sites between both surface types is significantly larger for magnesium (vide infra).

Bulk ^{35}Cl NMR. Despite the large surface areas, most of the chlorine (and magnesium) spins are still in sites with a bulklike conformation, where each magnesium is surrounded octahedrally by six chlorides. As a result, both ^{25}Mg and ^{35}Cl NMR spectra will be dominated by signal from the bulk or bulklike sites. The results of solid-state ^{35}Cl NMR measurements obtained at 15.625 kHz MAS at 20.0 T can be found in Figure 1A. It shows the central transition (CT) center band with two sets of spinning sidebands on both sides. For all samples, the CT only shows one component.

Compared to the neat material (dry MgCl$_2$), the sharp features of the quadrupolar powder pattern broaden and are smeared out. This has already been observed before for ball-milled MgCl$_2$[42] and is explained by a distribution in quadrupolar parameters that result from a disorder in the local environment. Such a distribution manifests itself in typical line shapes, such as the asymmetric broadening of the MAS spectra. The line shape is mainly the result of a distribution in quadrupolar parameters without much chemical shift broadening. This is most obvious examining the static experiments (Figure 1B), in which it can be seen that the discontinuity at the isotropic chemical shift position is present in all samples, while the two horns on the left and right are increasingly smeared out. The spectra of the binary adducts show the presence of larger distributions in quadrupolar parameters than those found for MgCl$_2$ DCM, which indicates a larger heterogeneity in these samples. This is not surprising given

the smaller particle dimensions. Along the sample series, as shown in Figure 1, there is a gradual increase in the distribution in quadrupolar parameters. The smallest particles with the highest donor loading (Do1_10 and Do3_7) give rise to the largest distribution in quadrupolar parameters.

^{35}Cl (and also ^{25}Mg) experiments were performed with long relaxation delays ($5 \times T_1$) and in the weak radio frequency (RF) regime ($\nu_{RF} \ll \nu_Q$) to ensure quantitative conditions and avoid line shape distortions.[45] Quantification of the spectral intensities (see Table 1) shows that the spectra of some samples lack a significant fraction of the anticipated signal. This is most prominent for the DMFluo (Do2) and DiBP (Do3) adducts, for which 10−20% of the ^{35}Cl signal is not detected. For Do3_7, a sample with a high donor loading and the smallest particle size, the largest fraction of ^{35}Cl signal escaped detection. It is also the sample with the least-defined line shape and thus the largest distribution in quadrupolar parameters. This loss of signal can pertain to sites with large quadrupole interactions, which consequently yield resonances that are broadened beyond detection (at least under the experimental settings used to acquire the spectra in Figure 1).

In general, there is a correlation between particle size (in the lateral dimension) and intensity loss in the chlorine Hahn-echo spectra (see Table 1). This strongly suggests that the surface sites in the lateral dimension are missing from the spectra. Such an observation is in agreement with the results from DFT calculations (vide infra) that predict large quadrupolar parameters for these surface sites, even after binding of donors. Remarkably, the samples containing DMDOMe (Do1) fall outside this trend (Figure 2). In particular, the spectrum of Do1_10 shows only a relatively low fraction of signal loss, despite a large surface area (small particle size), high donor loading, and a line shape showing a large distribution in quadrupolar parameters.

Line Shape. For neat ball-milled MgCl$_2$,[42] we previously described the distribution in quadrupolar parameters of the bulk-phase signal to be induced by surface effects (i.e., lack of long-range order) and fitted its line shape using the extended Czjzek distribution.[46,47] The much larger surface areas of the
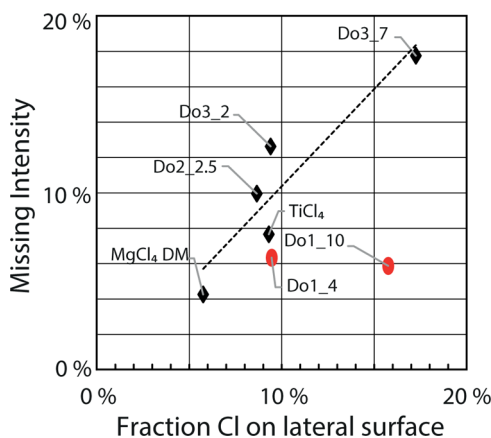
Figure 2. Missing intensity in quantitative ^{35}Cl NMR spectra vs fraction of Cl surface sites. ^{35}Cl intensities from solid-state NMR experiments are an average between MAS and static relative intensities, where the difference between MAS and static was never more than 3%.

smaller nanoparticles of the adducts explain the larger distribution in quadrupolar parameters observed.

The Czjzek model[48,49] can be used to describe a distribution in quadrupolar parameters for a disordered system. For systems with an intrinsic quadrupole moment, such as $MgCl_2$, a more elaborate model is necessary that can describe long-range disorder around a locally ordered site. For such situations, the so-called extended Czjzek model has been introduced.[46,47] Here, $C_{Q,0}$ and η_0 are the quadrupolar parameters for the well-defined first-order coordination sphere and, similar to the Czjzek model, the distribution in quadrupolar parameters caused by structural variations in the higher coordination spheres is described by the parameter σ.

A distribution in quadrupolar parameters as the result of ball milling was observed earlier by Bureau et al.[50] for GaF_3 and by Scholz et al.[51] for Al_2O_3. In both studies, the particle size is around 13 nm, very similar to what we obtain for neat ball-milled $MgCl_2$. In contrast to our ^{35}Cl spectra, bicomponent line shapes are observed, in particular for GaF_3. Because of a weak quadrupolar interaction in the ^{71}Ga spectrum prior to ball milling, the authors model their experimental spectra using two Czjzek distributions, with different σ-values. The site with the lowest σ is attributed to "crystalline grains" (i.e., bulk sites that are slightly more distributed than crystalline GaF_3), while the site with the largest σ is attributed to "grain boundaries" (i.e., surfaces). The latter corresponds to 70% of the intensity, showing that ball-milling impacts much more than just the outer shell. For Al_2O_3, Scholz et al. used a combination of Czjzek distribution and well-defined resonance to describe their spectra, again assigning the two components to grain boundaries/surfaces (referred to as "amorphous phase" in their contribution) and crystalline grains/bulk. The fraction of the amorphous phase even reaches 80%, again showing the far-reaching impact of ball milling. Just like $MgCl_2$, Al_2O_3 already has a quadrupolar interaction before ball milling and we therefore believe that an extended Czjzek model (which had not yet been introduced at that time) would be better suited to model the spectra of ball-milled Al_2O_3, in particular because the experimental spectrum shows no sign of two components (which clearly is the case in GaF_3). It is important to realize for our study that the ball milling affects a significantly larger fraction of the Mg and Cl sites in the nanoparticle than just

those in the outer shell. This is something which becomes apparent in the analysis of our relaxation data (vide infra).

We tried to describe our experimental line shapes using extended Czjzek distributions. Using the EGdeconv program,[52] the MAS spectra could be modeled reasonably well with a single component exhibiting an extended Czjzek distribution, as can be seen in Figure 3. The overall experimental line width
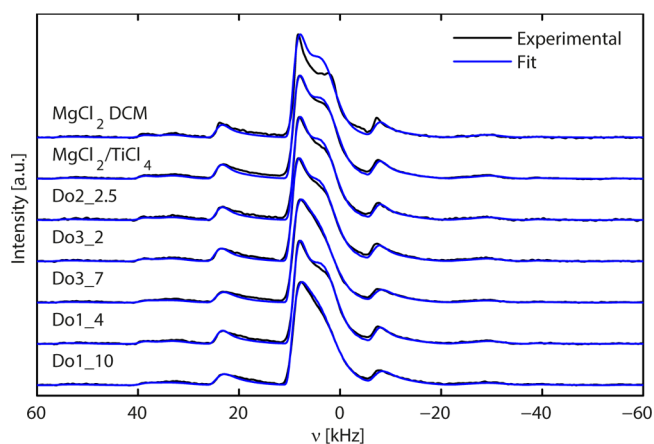

Figure 3. Fit of the ^{35}Cl MAS spectra ($B_0 = 20$ T) to the extended Czjzek model.

(in both the static and MAS spectra) does not increase along the sample series, despite the increasing distribution in quadrupolar parameters. The fitting results show that a larger distribution is compensated by a somewhat smaller $C_{Q,0}$, e.g., while the ^{35}Cl sites in neat $MgCl_2$ have a quadrupolar coupling constant, C_Q, of 4.61 MHz, adduct Do3_2 gives $C_{Q,0} = 4.36$ MHz and Do3_7 $C_{Q,0} = 4.16$ MHz (see Table 2). The

Table 2. Results from Fitting to the Extended Czjzek Distribution

samples code	$C_{Q,0}$ (MHz)	η_0	σ^a (MHz)
$MgCl_2$ DCM	4.34 ± 0.10	0.0	0.50 ± 0.05
$MgCl_2$/$TiCl_4$	4.46 ± 0.10	0.0	0.51 ± 0.05
Do2_2.5	4.36 ± 0.10	0.0	0.51 ± 0.05
Do3_2	4.36 ± 0.10	0.0	0.54 ± 0.05
Do3_7	4.16 ± 0.10	0.0	0.65 ± 0.05
Do1_4	4.40 ± 0.10	0.0	0.51 ± 0.05
Do1_10	4.22 ± 0.10	0.0	0.68 ± 0.05

^{a}Lower limit of the fitting routine is $\sigma = 0.5$ MHz.

decrease in C_Q can be attributed to the increased contribution of (001)-surface sites, which have slightly smaller quadrupolar coupling parameters compared to the bulk (see Table 3). For robustness, the fitting routine has a lower limit of 0.5 for the σ parameter. As a consequence, the actual distribution is slightly overestimated for some of the least disordered samples, in particular $MgCl_2$ DCM. The best agreement is found for the most disordered samples Do1_10 and Do3_7. Unfortunately, the static spectra could not be satisfactorily simulated using the parameters following from the MAS fit, nor could they be fitted properly to the extended Czjzek model (see Figure S2). It could be that some CSA is present in the static spectra, which prevents fitting them to a model only taking into account the quadrupolar interaction. Alternatively, even the extended Czjzek model may not be sophisticated enough to describe

Table 3. DFT Calculations of the ^{35}Cl and ^{25}Mg Quadrupole Parameters for Various Neat MgCl$_2$ Species and MgCl$_2$-H$_2$O Adducts, at B3LYP-D2/pob-TZVP Level

species	atom	^{35}Cl C_Q (MHz)	η	atom	^{25}Mg C_Q (MHz)	η
MgCl$_2$ bulk	Cl	4.4	0	Mg	1.62	0
MgCl$_2$(001)	Cl	4.9	0	Mg	1.51	0
MgCl$_2$(104)	Cl	15.0	0.7	Mg	11.2	0.3
	Cl$_{cs}$	6.7	0			
MgCl$_2$(110)	Cl	18.3	0.5	Mg	6.6	0.4
MgCl$_2$(104)−H$_2$O	Cl-1	10.5	0.7	Mg	2.3	0.8
	Cl$_{cs}$-2	5.7	0.9			
MgCl$_2$(110)−H$_2$O	Cl-1	19.7	0.4	Mg	10.5	0.1
	Cl-2	16.7	0.6			
MgCl$_2$(110)−2H$_2$O	Cl-1	13.6	0.3	Mg	6.5	0.6
	Cl-2	13.6	0.3			

the distribution that results from the effects causing both variation in first and higher coordination spheres of the chlorines. Although it would undoubtedly give a better fit, we do not think it is justified to include a second component into the fitting procedure, as was done in the studies of GaF$_3$ and Al$_2$O$_3$ because we see no features of a well-defined crystalline fraction (with pronounced quadrupolar features) in the spectra.

Relaxation. A strong reduction in the ^{35}Cl T_1 relaxation times is found for the binary adducts with respect to neat MgCl$_2$ (see Table S1). The relaxation times show a correlation with $\langle L_c \rangle$ in particular. In the following discussion of quadrupolar relaxation behavior, chlorine relaxation data are leading, as they are determined more reliably, but all conclusions appear to be valid for ^{25}Mg T_1 relaxation as well. Ball-milling neat MgCl$_2$ already has a small effect on the relaxation time and T_1 decreases further for the adducts. This suggests that fast relaxation is taking place at the surfaces, but also the relaxation rate of the bulk is increased as a result of local distortions. Due to the weak dipole−dipole interaction and the low natural abundance of, in particular ^{25}Mg, we exclude the option that spin diffusion governs the enhanced relaxation for the bulk. This is corroborated by the fact that the relaxation behavior under MAS is equal to that under static conditions.

The relaxation behavior of our particles can be fitted with a biexponential function, with the exception of neat MgCl$_2$, which shows monoexponential behavior. Although quadrupolar relaxation is intrinsically multiexponential; in practice, it is

often monoexponential for a spin $I = 3/2$,[53−55] in agreement with the relaxation behavior of neat MgCl$_2$. Therefore, the relaxation behavior of our binary adducts would suggest the presence of two phases, such as surfaces and bulk, each having its own typical relaxation. However, in the discussion about the distributed line shapes, we argued against such a distinction in two different phases because we find no evidence for a crystalline fraction. In analogy to a distribution in quadrupolar parameters to describe the observed line shape, a distribution in relaxation times seems more appropriate, and this can be modeled using a Weibull distribution ("stretched exponential"), as can be seen in Figure S3. Ideally, both distributions would even be connected, as $1/T_1 \propto \omega_Q^2$. Along the samples series, the distribution in ω_Q does not change dramatically, but T_1 times decrease drastically. Quadrupolar relaxation is often overwhelmingly dominated by fluctuating electric field gradients. This suggests that motion-driven relaxation processes play a crucial role and we hypothesize that defect-induced dynamics govern the fast relaxation. Surface sites have largest ω_Q (vide infra) and probably highest dynamics as well, resulting in the fastest relaxation. To fully understand the relaxation behavior, extensive field- and/or temperature-dependent relaxation measurements have to be performed, which is beyond the scope of this contribution.

The relaxation times of ^{25}Mg and ^{35}Cl appear to be strongly correlated. This again suggests that their relaxation is influenced by the same defect-induced dynamics. Mobility of donor molecules could also contribute to enhanced relaxation at the surfaces, but the reduction of T_1 for sample MgCl$_2$ DCM indicates that there is already enhanced relaxation in the absence of a donor.

DFT Calculations of ^{35}Cl Sites. The surfaces are, at least partially, covered by donor molecules. Intuitively, it would be expected that coordination of these molecules to the unsaturated (104)- and (110)-surfaces would have a large impact on the quadrupolar parameters. To interpret the quadrupolar NMR parameters, we calculated quadrupolar coupling constants (C_Q) and asymmetry parameters (η) for the binary adduct systems. As a test case to see if this hypothesis is true, we first calculated the ^{25}Mg and ^{35}Cl quadrupolar parameters for adsorbed water on the surface. We choose water because it is a small molecule with few degrees of freedom, as well as because water adsorption is known to occur in these kinds of samples. For the (110)-surface, binding of both a single water and a full coordinative saturation by the binding of two water molecules was considered (see Figure 4).
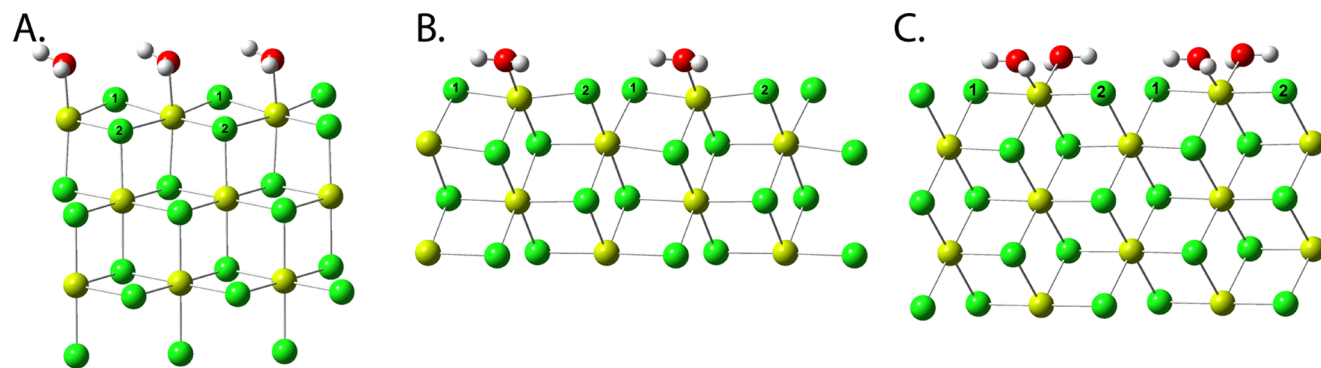

Figure 4. Optimized structures of H$_2$O (A) on the (104)-surface surfaces of MgCl$_2$ and (B, C) on the (110)-surface; Mg atoms are colored in yellow, Cl atoms in green, O atoms in red, H atoms in white. Cl-2 on the (104)-surface is in the Cl$_{cs}$ position.

Furthermore, we calculated quadrupolar parameters for $MgCl_2(110)-TiCl_4$, $MgCl_2(104)-DMDOMe$, and $MgCl_2(110)-DMDOMe$ adducts using periodic calculations. We used cluster models that were introduced in ref 34, for the calculations of the quadrupolar parameters for DiBP adducts and for a high-coverage model of DMDOMe. In the calculations, the donor molecules are coordinated in either the "bridge" or the "chelate" mode (see Figures 5, S8, and S9)
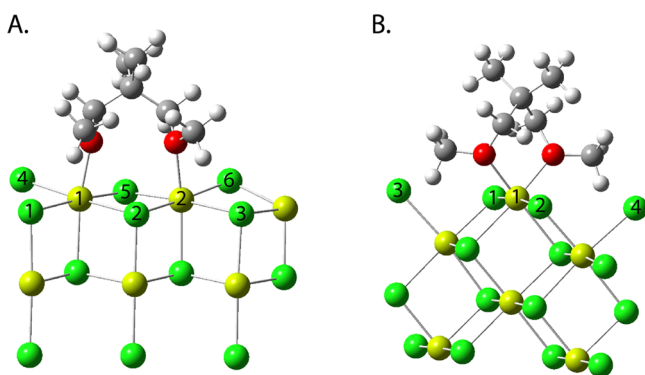

Figure 5. Optimized structures of DMDOMe on the surfaces of $MgCl_2$, showing a bridging conformation on the (104)-surface (A) and a chelating binding mode on the (110)-surface (B). For the sake of clarity, the picture shows only a few surface atoms close to the donor molecules; Mg atoms are colored in yellow, Cl atoms in green, O atoms in red, C atoms in gray, and H atoms in white.

and $TiCl_4$ adopts the so-called Corradini site (see Figure 6). For DMDOMe, also a monodentate coordination is considered to check the outcome for a pentacoordinated magnesium.
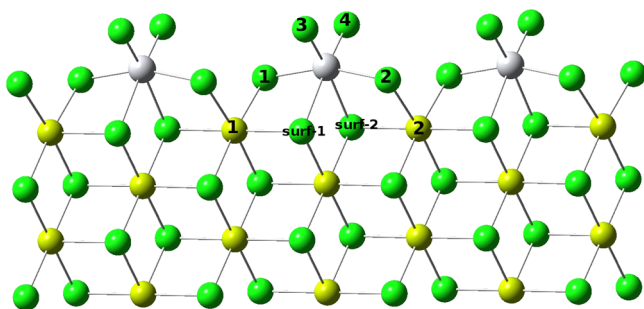

Figure 6. Optimized structures of $TiCl_4$ on the (110)-surfaces of $MgCl_2$; Mg atoms are colored in yellow, Cl atoms in green, and Ti atoms in gray.

The results of the calculations are summarized in Tables 3−6, and we will initially discuss the results concerning ^{35}Cl. As a reference, Table 3 also includes the quadrupolar parameters for exposed surface sites, which have been calculated before.[42] One addition is the inclusion of the (104)-Cl_{cs} sites. These correspond to chlorine sites on the (104) surface, which are bound to the unsaturated magnesium surface sites, but are coordinatively saturated (hence "cs") themselves. This sets them aside from the "real" surface chlorines that are bound to only two magnesium atoms; compare Cl-1 and Cl-2 in Figure 4A. The bulklike coordination of the Cl_{cs} sites is reflected in the C_Q, indeed being much closer to the bulk than to real surface sites. These Cl_{cs} sites have not been included in the calculation of the chlorine surface fraction in Table 1.

As expected, the quadrupolar parameters of the bare surface sites differ strongly from those of the bulk sites. The coordination of water has little effect on the ^{35}Cl quadrupole parameters of the surface sites, however. It does not really matter whether a pentacoordinated or hexacoordinated Mg site is formed or whether the (104)- or the (110)-surface is considered; in all situations, the ^{35}Cl C_Q of the surface sites remains very close to the values found for the bare surfaces. Only a small reduction in C_Q is observed for the Cl_{cs} sites.

Figure 5 shows structures of DMDOMe on $MgCl_2$. On the (104)-surface of $MgCl_2$, binding takes place via both oxygen in a bridging coordination and this restores the coordinative saturation of two surface magnesium sites, although no perfect octahedron is formed. The calculated quadrupole parameters at the B3LYP-D2/TZVP level are shown in Table 4. We note that for the bulk phase, slightly better agreement with experimental results was obtained at the B3LYP-D2/pob-TZVP level, although the results at the B3LYP-D2/TZVP level were comparable to this computational more demanding calculation. Moreover, the coefficients of the TZVP basis set were specifically optimized for $MgCl_2$ adducts[11] and hence we performed the calculations at the B3LYP-D2/TZVP level. Considering that we used slightly different approaches, we will mainly look at trends in the calculated C_Q values and do not focus too much on their absolute values. The results for the ^{35}Cl C_Q in the bridging coordination mode show no significant effect for Cl-4−Cl-6, while Cl-1−Cl-3 (Cl_{cs}) have again a reduced, bulklike C_Q-value. For binding of water, the most pronounced effect was observed for these Cl_{cs} sites as well. Also the coordination of DMDOMe to the (110)-surface does not affect the chlorine C_Q. There is hardly any difference between a monodentate and a chelating binding mode, similar to the case where water was considered.

The presented periodic calculations have some conceptual problems, as the small $MgCl_2$ nanoparticles lack long-range crystalline order. In ref 56, an alternative cluster description has been presented that should be better suited to describe such disordered systems. On the basis of this cluster approach, we proposed some high-coverage models[34] that were indeed found to better describe the $MgCl_2$−DMDOMe adducts as far as ^{13}C chemical shifts of the donor are concerned. Quadrupole parameters have been calculated for the optimized cluster model with three donors on the surface that has been shown in ref 34 and is reproduced in Figure S6. Two different conformers, namely, Do1**A** and Do1**C**, are considered and their presence have been indicated by ^{13}C NMR. For both conformations considered, this high-coverage cluster model does not result in significant changes in the chlorine quadrupole parameters and we report only the average ^{35}Cl C_Q. The conformation considered in the periodic calculation (chelate binding mode) corresponds to conformer Do1**C** from the cluster calculations.

Optimized cluster models for the DiBP donor in different conformation on both (104)- and (110)-surfaces were presented in ref 34 as well. The structures of these models are reproduced in Supporting Information Figure S7. The five different models consider a symmetric and an asymmetric conformation of the DiBP molecule on the two different surfaces. However, in none of the considered models, we find a significant effect of donor coordination on the ^{35}Cl C_Q for the surface sites (Cl-4−Cl-6) (see Table 5). These results are in line with the other calculations and indicate that the quadrupolar parameters of surface chlorines are insensitive to

Table 4. DFT Calculations of the ^{35}Cl and ^{25}Mg Quadrupole Parameters for MgCl$_2$(104)−DMDOMe and MgCl$_2$(110)−DMDOMe Adducts, at B3LYP-D2/TZVP Level

species	atom	^{35}Cl C_Q (MHz)	η	atom	^{25}Mg C_Q (MHz)	η
MgCl$_2$(104)−DMDOMe	Cl-1	6.1	0.3	Mg-1	2.81	0.3
	Cl-2	4.2	0.0	Mg-2	2.91	0.3
	Cl-3	6.0	0.3			
	Cl-4	11.1	1.0			
	Cl-5	12.1	1.0			
	Cl-6	11.2	0.1			
MgCl$_2$(110)−DMDOMe monodentate	Cl-1	13.5	0.4	Mg-1	11.9	0.2
	Cl-2	15.2	0.5			
	Cl-3	14.9	0.6			
	Cl-4	15.1	0.6			
MgCl$_2$(110)−DMDOMe chelate	Cl-1	13.5	0.5	Mg-1	3.42	0.7
	Cl-2	13.4	0.6			
	Cl-3	14.9	0.5			
	Cl-4	14.8	0.6			
high-coverage clu_27u_110 3Do1**A**	Cl	13.1	0.6	Mg-l	2.1	0.7
				Mg-m	1.8	1.0
				Mg-r	2.2	0.9
high-coverage clu_27u_110 3Do1**C**	Cl	13.5	0.6	Mg-l	3.2	0.6
				Mg-m	2.9	0.9
				Mg-r	3.2	0.6

Table 5. DFT Calculations of the ^{35}Cl and ^{25}Mg Quadrupole Parameters for MgCl$_2$−DiBP Adducts, from Cluster Calculations

species	atom	^{35}Cl C_Q (MHz)	η	atom	^{25}Mg C_Q (MHz)	η
clu_24u_110 Do3**S**	Cl-1	6.1	0.4	Mg-1	1.8	0.4
	Cl-2	3.2	0.7	Mg-2	1.8	0.4
	Cl-3	6.1	0.4			
	Cl-4	10.8	1.0			
	Cl-5	13.3	0.4			
	Cl-6	10.8	1.0			
clu_24u_110 Do3**A**	Cl-1	5.4	0.2	Mg-1	2.0	0.8
	Cl-2	4.9	0.8	Mg-2	2.1	0.6
	Cl-3	5.9	0.3			
	Cl-4	11.6	1.0			
	Cl-5	12.6	0.8			
	Cl-6	11.0	0.9			
clu_24u_110 Do3**A1**	Cl-1	5.7	0.4	Mg-1	2.5	0.9
	Cl-2	5.6	0.6	Mg-2	1.7	0.9
	Cl-3	5.5	0.2			
	Cl-4	11.4	1.0			
	Cl-5	12.0	0.8			
	Cl-6	12.0	1.0			
clu_27u_110 Do3**S**	Cl-1	13.3	0.5	Mg-1	2.5	0.6
	Cl-2	13.9	0.4			
clu_27u_110 Do3**A**	Cl-1	13.9	0.5	Mg-1	2.6	0.5
	Cl-2	13.4	0.5			

binding of molecules. After binding, the chlorines in the Cl$_{cs}$ position (Cl-1−Cl-3) have their C_Q reduced from 6.7 MHz toward the bulk value, in agreement with the other calculations. The chelating coordination of DiBP on the (110)-surface of MgCl$_2$ also restores the coordinative saturation for magnesium. However, the surface chlorines Cl-1−Cl-2 again yield C_Q values close to the bare surface chlorines and appear to be only marginally influenced, in both the symmetric and asymmetric conformers.

Some effects on the chlorine quadrupolar parameters are seen for the binary system MgCl$_2$−TiCl$_4$ (see Table 6). In

Table 6. DFT Calculations of the ^{35}Cl and ^{25}Mg Quadrupole Parameters for MgCl$_2$(110)−TiCl$_4$, at the B3LYP-D2/pob-TZVP Level

species	atom	^{35}Cl C_Q (MHz)	η	atom	^{25}Mg C_Q (MHz)	η
B3LYP-D2/TZVP	Cl$_{surf}$-1	8.9	0.6	Mg-1	2.05	0.7
	Cl$_{surf}$-2	8.9	0.6	Mg-2	2.05	0.7
	Cl-1	17.8	0.1			
	Cl-2	17.8	0.1			
	Cl-3	21.1	0.8			
	Cl-4	21.1	0.8			

particular, the two chlorine surface sites that are directly involved in TiCl$_4$ coordination (see Figure 6) are calculated to have a reduced C_Q (from 18 to 9 MHz), although it remains significantly large. The other chlorine atoms (Cl-1−Cl-4) are exclusively bound to Ti. They are calculated to have C_Q values of 18 and 21 MHz, which are in the same order of magnitude as, or even larger than, the exposed MgCl$_2$ surfaces. The observation of the titanium-bonded chlorines with solid-state NMR suffers therefore from the same difficulties as observation of the surface sites: both belong to diluted species and will give very broad lines and hence are difficult to observe in the bulk MgCl$_2$-dominated spectrum. Johnston et al.[57] showed a ^{35}Cl solid-state NMR spectrum for TiCl$_4$ grafted on SiO$_2$, an experiment that obviously benefits from the lack of a chlorine-containing substrate. They observed a ~400 kHz broad pattern and simulated that with C_Q = 14.3 MHz and η = 0.15, which seem in line with our calculations for the titanium-bonded chlorides. However, it should be noted that the coordination mode of TiCl$_4$ on SiO$_2$ is different from the coordination mode on MgCl$_2$.

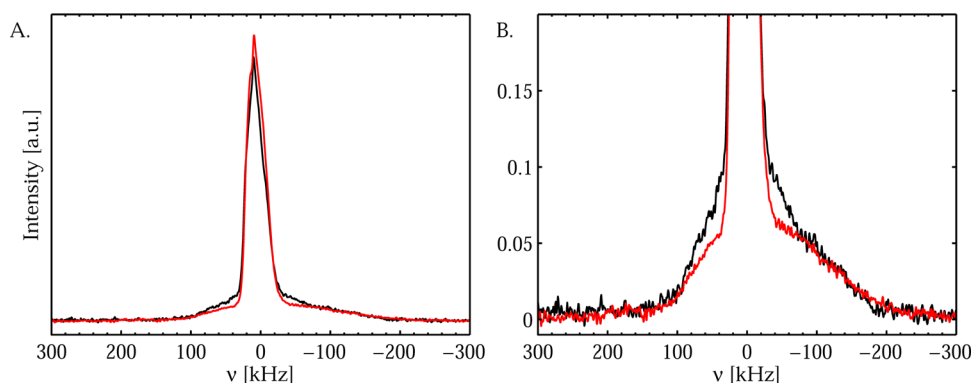Our calculations of the ^{35}Cl quadrupolar coupling parameters show that they are hardly affected by various

Figure 7. (A) Static ^{35}Cl NMR spectra of MgCl$_2$ Do1_10 (black) and Do3_7 (red) obtained at B_0 = 18.8 T and 500 kHz RF. (B) Zoom of the surface site, cutoff vertical scale at 0.20.

donor molecules and coordination modes. In some cases, η changes slightly, but in all considered structures (for both (104)- and (110)-surfaces), the ^{35}Cl C_Q appears to be unperturbed by surface binding of donor molecules, with the exception of chlorines coordinating to TiCl$_4$ and chlorines in the Cl$_{cs}$ position. In our previous study, the Cl$_{cs}$ position was not primarily considered as a surface site because it has, in first approximation, a bulklike coordination. Similar to the (001)-surface, it should therefore have quadrupole parameters similar to the bulk. In the case of an uncoordinated surface, its parameters are calculated as C_Q = 6.7 MHz and η = 0. After coordination of donors, the quadrupolar parameters for the Cl$_{cs}$ sites are almost restored to bulk values. The ^{35}Cl C_Q for the real surface sites are hardly influenced by absorption of a donor on either the (104)- and (110)-surface and still yield large C_Q (<12 MHz). Hence, these chlorine sites remain "invisible" also after coordination of a donor. Consequently, the loss of intensity in the chlorine spectra could therefore still pertain to distorted surface sites, similarly to what has been found for the bare surfaces in MgCl$_2$ DCM. The low signal loss for Do1_10 suggests the formation of surface sites with a smaller ^{35}Cl C_Q. However, the calculations of the ^{35}Cl C_Q for the proposed chelating binding mode on a (110)-surface give large C_Q values, suggesting that different structural models should be considered, e.g., relating to specific defects generated as a result of the ball-milling process.

^{35}Cl NMR Spectra of Surface Sites. The single resonance that is observed in ^{35}Cl spectra is assigned to the bulk phase of the MgCl$_2$ nanoparticles, although it might also include contributions from well-defined surface sites such as (001)-terminations. The signal from surface sites is not observed in Figure 1A or B because it is broadened beyond detection as follows from the calculated quadrupolar parameters. In an attempt to observe and characterize these surface sites with large C_Q, we acquired rotor-synchronized sideband-selective double-frequency sweep quadrupolar Carr−Purcell−Meiboom−Gill (ssDFS-QCPMG) (MAS) and QCPMG (static) spectra to increase sensitivity. In the case of ^{25}Mg spectra (vide infra), these methods allowed the detection of additional signal, but in ^{35}Cl, we did not observe a second signal, while we did get some line shape distortions (see Figures S4 and S5).

In a previous publication[58] we showed that the use of high-RF fields, which enable broadband excitation, makes broad resonances visible for Do1_10. Using a static home-built probe with a 1.2 mm inner diameter coil, we reached an RF field strength of 500 kHz for ^{35}Cl at a static magnetic field strength

of 18.8 T (ν_L = 78.3 MHz). We showed that this led to the detection of part of the satellite transitions from the MgCl$_2$ bulk, but also to the observation of signal from the surface sites, which will be discussed in more detail here. Using nutation NMR and variable offset cumulative spectra, we showed the absence of other, much broader, components for Do1_10. The high RF experiment is now also applied for Do3_7 and MgCl$_2$ DCM. Figure 7 compares the spectra of Do1_10 and Do3_7, where clearly a ~350 kHz broad resonance is detected for both adducts. The control experiment for MgCl$_2$ DCM gives a flat baseline.

For both samples, the resonances show a somewhat asymmetric line shape, but they do not show well-defined quadrupolar features. This suggests the presence of a distribution in quadrupolar parameters, which is expected given the supposed heterogeneous nature of the surfaces. The two samples do give distinctly different spectra, where Do1_10 appears to give additional signals compared to Do3_7. The experiments at high-RF field are not performed under quantitative conditions, prohibiting the ability to retrieve absolute intensities. Nevertheless, the spectra in Figure 7 can still be interpreted semiquantitatively, given that the sample amount (± 1 mg) and relative MgCl$_2$ content of the samples are very comparable. This shows that Do1_10 has more intensity in the broad signals. For Do3_7, there are two signals: besides the bulk phase signal, there is one broad resonance spanning about 350 kHz that should result from a surface site. After comparison with Do3_7, it becomes clear that the spectrum of Do1_10 actually has three resonances. Besides the bulk phase signal and the ~350 kHz broad resonance, there is also a less intense resonance spanning about 170 kHz. From the span of this resonance, a C_Q of ~8 MHz is estimated, which is significantly smaller than any of the calculated C_Q values.

An ~350 kHz broad resonance corresponds to a C_Q of ca. 10−11 MHz. Although a bit lower, this is in the range of calculated C_Q's for the surfaces (ca. 12−14 MHz, whether coordinated with donors or not, Tables 3−5). As none of the adducts have a full surface coverage of the donor, uncoordinated surface sites remain present for both Do1_10 and Do3_7. We can therefore not be certain whether the signal in the spectrum of Do3_7 originates from exposed or coordinated surface sites or both. For Do1_10, the ~350 kHz broad resonance corresponds most likely to exposed surface sites. A T_1 measurement for Do3_7 under the high ν_{RF} conditions shows that the ~350 kHz broad surface site has a
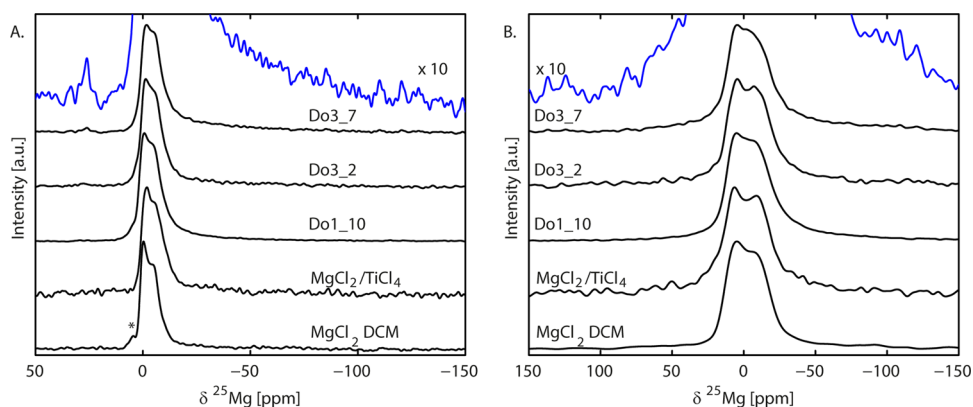
Figure 8. (A) ^{25}Mg rotor-synchronized Hahn-echo NMR spectra of selected $MgCl_2$ binary adducts obtained at MAS speeds of 10 or 15.625 kHz, $B_0 = 20$ T. The shoulder observed on the left-hand side of the main resonance in some of the spectra (marked by an asterisk for DCM) originates from the satellite transitions. (B) Static ^{25}Mg Hahn-echo NMR spectra of selected $MgCl_2$ binary adducts. The top spectra in blue are a 10× enlargement of $MgCl_2$ Do3_7 emphasizing the broad component.

short T_1: spectral integration of part of this signal, outside the span of the bulk signal, shows a monoexponential behavior with a T_1 of around 10 ms. The combination of large ω_Q and dynamics at the surface can explain this short relaxation time of the surface sites. It is remarkable that no broad signal is observed for $MgCl_2$ DCM at all, as this has surface sites ($\pm 5\%$) as well. We do note that weak X-band electron paramagnetic resonance signals are observed for $MgCl_2$ DCM, indicating the presence of some radicals, which are most likely formed during ball milling. These sites could induce very fast relaxation, which can explain the absence of detectable surface sites for the ball-milled samples. We consider potential radical sites to be quenched in the presence of donors.

The calculations indicate only small effects of donor coordination on the ^{35}Cl quadrupolar parameters and consequently the difference between both donors should be small. However, this is not in line with the ^{35}Cl visibility (Table 1). Also, the high ν_{RF} experiments are not in agreement with this, as is clear from the detection of the additional resonance with reduced C_Q for Do1_10. Both experiments suggest that for Do1_10 a surface structure is formed, in which the surface chlorines are affected by the donor coordination in such a way that their C_Q becomes lower (8 MHz), explaining both the observed additional resonance as well as the relative high ^{35}Cl visibility for this sample. This particular surface construct is consequently different from the suggested models as the C_Q calculated for the models are too high. The high-coverage model 3Do1A has shown good agreement with experimental ^{13}C NMR results, however giving rise to some inconsistencies. More evidence of the surface structures might follow from the calculation of ^{25}Mg C_Q and the detection of surface sites via ^{25}Mg NMR.

Bulk ^{25}Mg NMR. While ^{35}Cl is considered an insensitive nucleus, the sensitivity of ^{25}Mg NMR is generally even lower due to its lower gyromagnetic ratio and low natural abundance. Nevertheless, ^{25}Mg NMR might be more sensitive to changes on the surface because it should be directly involved in the binding of the donors. ^{25}Mg Hahn-echo spectra for selected adducts are shown in Figure 8A. Again, the quadrupolar powder pattern features are most pronounced in $MgCl_2$ DCM, but the line shapes look rather comparable for all samples. Also in the static spectra (see Figure 8B) the signal is rather similar for all samples with comparable levels of distribution in the quadrupolar parameters. This is in contrast to the ^{35}Cl

measurements, where there was a clear difference in the level of distribution in quadrupolar parameters for the different samples. The larger the distribution, the less well-defined the line shapes get and the longer the observed tailing of the signal. However, the ^{25}Mg C_Q (≈ 1.65 MHz) is much smaller than the ^{35}Cl C_Q.

The ^{25}Mg MAS spectra indicate the presence of additional site(s), which show up as a pronounced tailing on the right-hand side and actually differs significantly between the samples. The strongest tailing, and thus the largest distribution in quadrupolar parameters, is observed for Do3_7 and it stretches out as far as −8 kHz (−150 ppm), as is shown in the blown-up top trace in Figure 8A. A significant tailing is also observed for Do3_2 and $MgCl_2$/$TiCl_4$, stretching to ca. −5 kHz (−100) ppm. For $MgCl_2$ DCM and Do1_10, the asymmetric line is more narrow and slopes down to −2.5 and −4 kHz (ca. −50 and −75 ppm), respectively. In the static spectra, there are clues for the presence of a broader component as well, as can be seen in the rescaled top trace in Figure 8B. Again, this underlying component is broadest for Do3_7.

Spectral overlap makes it difficult to exactly identify this second component. An experiment that might help to alleviate this issue is the multiple-quantum MAS (MQMAS) experiment[59,60] thanks to its ability to separate overlapping quadrupolar broadened resonances in a two-dimensional fashion. Unfortunately, we were not able to observe the second site in MQMAS experiments (see Figure S8) due to the limited RF field strength (ν_{RF}), which hampers the excitation and conversion of the triple-quantum coherence.

Similar to the fraction of chlorine surface sites, the fraction of magnesium surface sites can be estimated from the particle dimensions. In contrast to the chlorine case, the fraction of magnesium surface sites differs a lot between the (104)- and (110)-surfaces. Particles having mostly (104)-surfaces expose 60−70% more surface sites than the equisized particles exhibiting (110)-surfaces (see Table 1). For example, if it would exhibit (104)-surfaces, the Do3_7 adduct would feature 31% surface sites, compared to 19.5% in case it exhibits (110)-surfaces. The difference between both surfaces might therefore seem to be an easy handle to interpret the ^{25}Mg spectra. However, the quadrupolar couplings of the coordinated surfaces are much closer to the bulk value (vide infra), meaning that surface sites should not be broadened beyond detection in ^{25}Mg spectra and they might significantly overlap
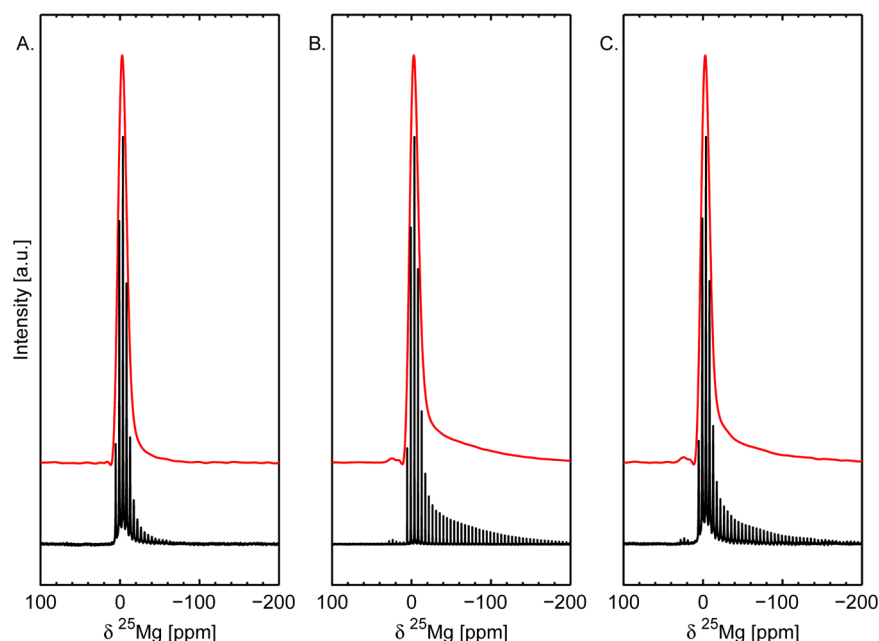
Figure 9. Rotor-synchronized ^{25}Mg ssDFS-QCPMG NMR spectra of selected MgCl$_2$ binary adducts: (A) Do1_10, (B) MgCl$_2$/TiCl$_4$, and (C) Do3_7, B_0 = 20 T.

with the bulk. On the other hand, only a part of the surface sites is actually covered with donors. Exposed surface sites with large quadrupole parameters are still present as well. For reasons not fully understood, the magnesium intensities from Figure 8 could not be reliably determined. Although the spectral quality appears high enough, no consistent magnesium intensities were found. Both spectral integration as well as the FID maximum did not result in reproducible relative intensities over different measurement sessions.

DFT Calculations of ^{25}Mg Sites. Binding of donor molecules to the unsaturated (104)- and (110)-surfaces restores coordinative saturation which will (partially) recover local symmetry. It is therefore expected to have more pronounced impact on the quadrupolar parameters for magnesium than what was found for chlorine. The binding of molecules has indeed various effects on the calculated quadrupole parameters for ^{25}Mg, as tabulated in Tables 3−6. The extent to which C_Q is reduced varies between the different models and coordination modes. For example, the interaction with water (see Table 3) leads to a significant reduction of ^{25}Mg C_Q when octahedral coordination is restored. Moreover, there is a significant difference between the (104)- and (110)-surface. The coordination of a single water on the (110)-surface, giving a pentacoordinated magnesium, also has an effect on the C_Q, but it remains large (<10 MHz).

The bridging coordination of DMDOMe on (104)-surfaces leads to restoration of coordinative saturation. The consequence is a strongly reduced C_Q for both coordinated magnesium sites, with values that approach the bulk (see Table 4). On the (110)-surface, the ^{25}Mg C_Q is strongly reduced as well, but only in the case of a chelating binding mode. The monodentate binding of DMDOMe on (110) gives similar results to the coordination of a single water where the C_Q remains large.

High-coverage models, which we introduced in ref 34, allowed for a better description of the system, based on a comparison of the ^{13}C chemical shifts. Comparing the quadrupolar parameters of the high-coverage model to a single

donor model shows interesting differences for ^{25}Mg C_Q (Table 4) again in contrast to the chlorides where no effect was observed. We focus on the central Mg site (Mg-m) as this should be most representative, although the results are actually rather comparable to the left- and right-hand-side Mg sites. Interestingly, the exact conformation considered in the high-coverage model is of significant influence on the ^{25}Mg C_Q. On the basis of ^{13}C chemical shifts, Do1A was identified as the sole conformer in Do1_10 and the major component in Do1_4. This conformer yields a C_Q that is very close to the bulk value of 1.65 MHz. Do1C, which was found to be present as a minor component in Do1_4, gives a C_Q of 2.9 MHz, again a strong reduction compared to the bare surface, but significantly larger than Do1A. These differences should result in significant differences in the line widths of the respective resonances.

In the case of the bridging coordination of DiBP (Do3) on the (104)-surface of MgCl$_2$, also coordinative saturation is restored. This is directly reflected in the quadrupolar parameters for the two involved surface magnesium sites (see Table 5). Remarkably, conformer A1 appears to induce a difference between the two Mg surface sites, while conformer A does not. All in all, in both the symmetric and asymmetric conformers, C_Q is strongly reduced to values close to the bulk C_Q. The chelating coordination of DiBP on the (110)-surface of MgCl$_2$ leads to a reduction of ^{25}Mg C_Q as well. Again octahedral coordination is restored and thus the corresponding C_Q shows a significant reduction, but appears to be slightly larger than at the (104)-surface (see Table 5). Also in this case there is no significant difference between the symmetric and asymmetric conformers.

The MgCl$_2$−TiCl$_4$ binary adducts show pronounced effects on the ^{25}Mg C_Q as well (see Table 6). Binding of TiCl$_4$ generates magnesium surface sites with an octahedral coordination by chloride ligands, very similar to the bulk, although this is only true for a high TiCl$_4$ loading. At lower loadings, the resulting Mg sites will be pentacoordinated. Alternatively, TiCl$_4$ molecules might coordinate on steps or holes[9,56] with structures locally resembling the structural

motive, as shown in Figure 6, so that for at least one of the two magnesium sites octahedral coordination is restored. C_Q for the octahedral magnesium sites comes down to approximately 2 MHz, which is very close to the bulk value. The results are in line with the results from the donors, but this is the only case where the binding does not take place to an oxygen, but to a chlorine.

Our calculations of the ^{25}Mg quadrupolar parameters show that they are affected to a different extend by various coordination modes. Coordination of one oxygen to the (110)-surface (a single H_2O or monodentate coordination of a donor), leading to pentacoordinated magnesium, already lowers ^{25}Mg C_Q, but it remains significantly higher than in the case of hexacoordinated magnesium. In all considered structures (for both (104)- and (110)-surfaces), ^{25}Mg C_Q reduces strongly after restoration of the octahedral surrounding with both oxygen and chlorine ligands. In the case of $MgCl_2-H_2O$ and $MgCl_2-$donor adducts, ^{25}Mg C_Q generally becomes 2−6 MHz, but only when octahedral coordination is restored. Despite a clear reduction compared to the exposed surfaces, the resulting C_Q generally remains somewhat larger than the bulk. The high-coverage model 3Do1**A** on the (110)-surface results in the largest reduction of C_Q for the covered surfaces and it almost reaches bulk values.

^{25}Mg NMR Spectra of Surface Sites. The calculated quadrupole coupling constants of coordinated magnesium surface sites (2−4 MHz) correspond to resonances with line widths (3−18 kHz at 20.0 T) that should be detectable under regular conditions. However, sensitivity could be an issue because only a small fraction (2−10%) of the spin pool is a covered surface site. ^{25}Mg Hahn-echo experiments already showed the presence of additional components. To increase the sensitivity of ^{25}Mg NMR experiments, we obtained static QCPMG and ssDFS-QCPMG spectra under MAS. The ssDFS sequence[61] gave enhancements in the S/N ratio of up to ∼2.7. The ssDFS-QCPMG experiments actually emphasize the broad signal on the right-hand side over the bulk phase signal. Moreover, the spikelet spectrum allows for an easy differentiation between baseline and the broad components of the signal. Due to increased sensitivity, the tailing is observed to span an even larger frequency range compared to the spectra in Figure 8. For TiCl$_4$ and DiBP adducts, the signal extends beyond −10 kHz (−200 ppm). For the Do1_10 sample, it only tails to −5 kHz (−100 ppm, see Figure 9). The broad signal lacks well-defined features, and the asymmetric featureless tailing is again indicative of a distribution in quadrupolar parameters reflecting disorder.

Also in static QCPMG experiments, the additional broader component can easily be detected in the spikelet spectrum. The sensitivity for static QCPMG experiments could be boosted with a double-frequency sweep (DFS) prepulse, giving enhancements of ∼2.9 for DCM, Do1_10, and Do3_7 with line shapes similar to the experiments without DFS (see Figure S9). Clearly, this second broad component is detected for most samples, but not for Do1_10 (see Figure S10). Generally, the relative intensities in the QCPMG spectrum are the same as in a spectrum obtained by a Hahn echo, with the exception of Do1_10, where the QCPMG spectrum is actually narrower than that obtained by Hahn echo. For that sample, the Hahn echo shows some broadening due to a distribution in quadrupolar parameters, but this is not very apparent in the QCPMG spectrum.

The DiBP adduct with the smallest particles (Do3_7) gives the broadest QCPMG spectrum, spanning almost 25 kHz (from ∼200 to −250 ppm). Additional QCPMG experiments were performed at higher ν_{RF} of 20 kHz for this sample. This is no longer in the low ν_{RF} nutation regime for the signal of the bulk phase ($C_Q \approx 1.65$ MHz). Therefore, it led to some line shape distortions as well as signal loss for the narrow signal. The signal intensity of the broader component is very similar in both experiments. Importantly, the higher ν_{RF} did not lead to the excitation of further, even broader, resonances (see Figure S11). QCPMG experiments were also performed at a second magnetic field strength of 14.1 T. At the lower field, the line widths naturally increase due to stronger quadrupolar broadening. However, after scaling the axis for the field difference, the spectra for 14.1 and 20.0 T can be overlaid and show identical line shapes. This proves that the line shapes of the resonances are purely of quadrupolar origin.

The additional resonances that are detected have significant intensities, which impose some problems. Due to the potential difference in T_2 between different components, QCPMG experiments are in first approximation no longer quantitative. However, comparison between the first echo and the sum of all echoes shows only small difference in the line shape and thus relative intensities comparable to a single Hahn echo. The high intensity of the broad resonances can therefore not completely be explained by T_2 effects. For Do3_7, the broad component corresponds to a much larger fraction of the signal than can be accounted for by the donor loading. Also, calculated C_Q's of ca. 2−2.5 MHz are actually too small to account for the observed span of the resonance, in particular if we consider that larger ν_{RF} might give somewhat broader lines. This is also true for the TiCl$_4$ adduct, the C_Q of the surface magnesium for the TiCl$_4$ adduct is calculated as 2 MHz (Table 6). This value underestimates the width of the experimental spectrum, which indicates a C_Q of up to ∼3.5 MHz. These differences might be related to the accuracy of the calculations. Also here, the second site represents much more spins than the 8% that can account for TiCl$_4$-bound sites (since per TiCl$_4$, there are two surface chlorine sites involved in the binding). On the basis of relaxation data, we concluded earlier that the surfaces might affect a much larger fraction of the spins than just the outer shell, e.g., due to defects caused by the milling process.

For Do1_10, no broad component is detected, suggesting that the quadrupolar parameters of covered surface sites are very close to the bulk and those sites will (practically) overlap. This is in agreement with the C_Q value (1.8 MHz) calculated for Do1**A**, which is the main surface structure, as followed from ^{13}C experiments. However, ^{35}Cl NMR results suggest a different surface construct. For Do1_4, on the other hand, a second surface structure was identified using ^{13}C NMR: Do1**C**, for which a larger quadrupole parameter of 2.9 MHz is predicted. The presence of Do1**C** can explain the second site that is indeed found in the QCPMG experiments for this sample. In fact, the calculated quadrupolar parameters match the experimental span, although the accuracy of the calculations does not allow for such a specific agreement. Again, there is a problem with the intensities though. The ^{13}C NMR results indicate that Do1**C** is only a minor component[34] and it can therefore not account for such an intense signal.

Donor−Surface Interactions. Since the surfaces are covered with organic donors and thus with protons, this should offer the possibility to do correlation experiments between the donors and the surface sites. To this end, we
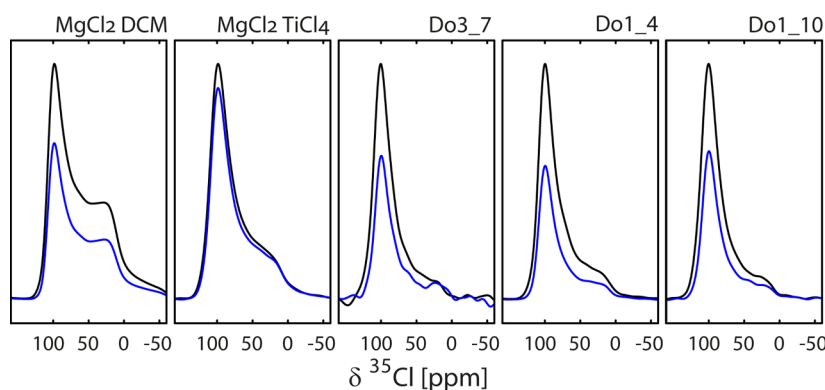
Figure 10. Results of $^{35}Cl-\{^{1}H\}$ ssDFS-REDOR-QCPMG experiments for $MgCl_2$ adducts obtained at 15.625 kHz MAS, $B_0 = 20$ T. The black lines are the reference spectra (S_0), while the blue lines are the REDOR spectra (S) at a REDOR time of 65 ms.
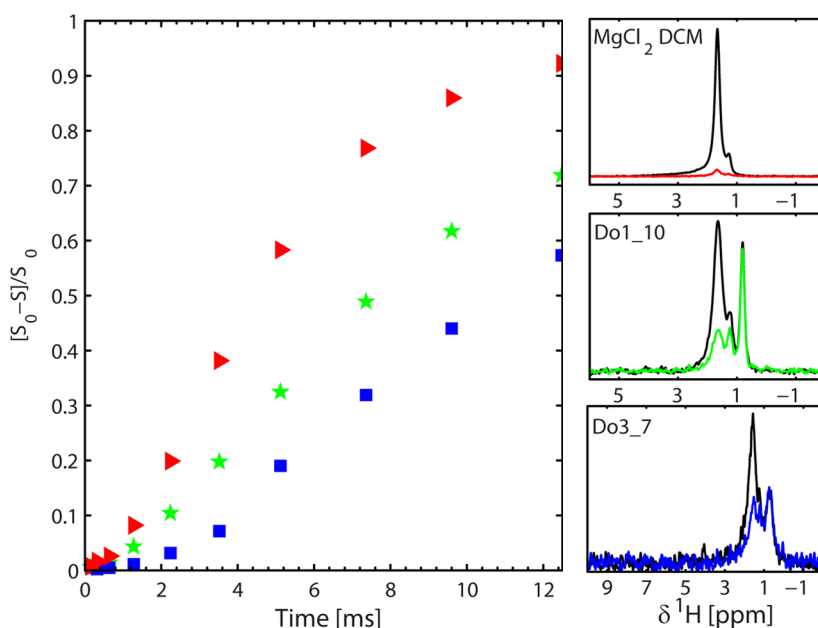

Figure 11. TRAPDOR curve of $^{1}H-\{^{35}Cl\}$ TRAPDOR experiment for $MgCl_2$ DCM (full spectrum, red triangles), Do1_10 (Mg−OH signal, green stars), and Do3_7 (Mg−OH signal, blue squares). The right column shows spectra after 12.5 ms dephasing time, where the black lines are the reference spectra (S_0) and colored traces are the TRAPDOR spectra (S). MAS speed = 12.5 kHz, ν_{RF} ^{35}Cl = 30 kHz.

performed $^{1}H-^{35}Cl$ and $^{1}H-^{25}Mg$ double-resonance experiments to probe potential interactions.

$^{1}H-^{35}Cl$ Correlation Experiments. $^{1}H-^{35}Cl$ cross-polarization (CP) experiments were employed with the aim to selectively get signal for those sites in the vicinity of donors (i.e., surface sites) and suppress the signal from the bulk phase. However, the resulting $^{1}H-^{35}Cl$ CP spectra showed signals very comparable to the direct excitation (see Figure S12). Moreover, these measurements proved to be very time-consuming because of low CP efficiencies[62] and also because ^{1}H T_1 times (2−3 s) are significantly longer than the T_1's of the quadrupolar nuclei (150 ms for smallest nanoparticles).

$^{35}Cl-\{^{1}H\}$ REDOR and $^{1}H-\{^{35}Cl\}$ TRAPDOR experiments have been performed to get a deeper insight into the donor−surface interactions. The REDOR sequence has been combined with signal enhancement schemes to give an ssDFS-REDOR-QCPMG pulse sequence for enhanced sensitivity. $^{35}Cl-\{^{1}H\}$ REDOR experiments show a clear Cl−H interaction (see Figure 10). The REDOR fraction reaches 40% for most of the samples after a dephasing time of ~65 ms.

This includes the $MgCl_2$ DCM sample, which has no donor protons. Previously, we did observe that this sample contains Mg−OH groups.[42] The other donor-free adduct, $MgCl_2-TiCl_4$, only reaches a REDOR fraction of 11%, thus clearly having less or weaker Cl−H dipolar interactions.

Due to the relative high natural abundance (75%) of ^{35}Cl, it should be possible to perform the reverse experiment, $^{1}H-\{^{35}Cl\}$ REDOR, to get more insight into the protons responsible for the observed Cl−H REDOR effect. Due to the strong ^{35}Cl quadrupole interaction, the REDOR-type experiment is not feasible, but alternatively a $^{1}H-\{^{35}Cl\}$ TRAPDOR can be used as shown in Figure 11. The ^{1}H spectrum of $MgCl_2$ DCM shows a sharp signal at 1.66 ppm, which has been assigned to a Mg−OH surface group.[42,63−65] This signal shows a clear TRAPDOR effect. After 12.5 ms of chlorine irradiation, the TRAPDOR effect, $\Delta S/S_0$, is 95%. The broad signal around 4 ppm, most likely related to some H_2O, has a much shorter T_2, but shows a TRAPDOR effect as well. In $MgCl_2-TiCl_4$, there is also a pronounced TRAPDOR effect, again for the signal at 1.66 ppm as well as the signal at 3.8 ppm (most likely some H_2O-related signal), as shown in Figure S13.
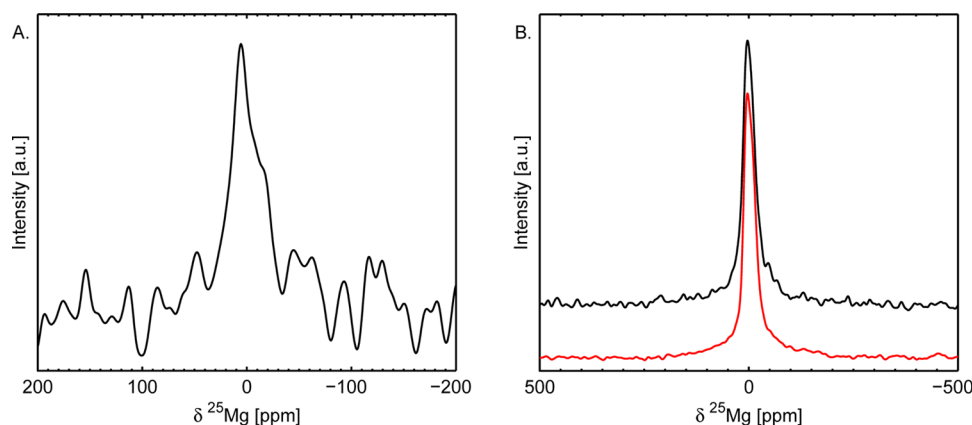
Figure 12. (A) Static $^1H-^{25}Mg$ CP spectrum of $MgCl_2$ DCM (room temperature) and (B) comparison of the $^1H-^{25}Mg$ CP spectrum (black, -40 °C) of Do3_7 to a QCPMG spectrum (red, room temperature), $B_0 = 20$ T.

The proton spectrum shows two resonances at 1.26 and 0.84 ppm that can be assigned to hydrocarbons physisorbed to the $MgCl_2$ particles. These narrow signals have a long T_2 and dominate the ^1H spectrum at longer echo times, but clearly do not show any TRAPDOR effect.

The signals from physisorbed hydrocarbons and Mg–OH are also the relevant proton signals in the TRAPDOR experiments of the DMDOMe (Do1) adducts. The signals from the donor have a short T_2 (and are therefore not visible in the spectra for Do1_10 in Figure 11) as they have decayed before any TRAPDOR effect could be observed. What is left at longer dephasing times are again hydrocarbon signals that do not show any TRAPDOR effect and a Mg–OH peak with a relatively strong TRADPDOR effect (see Figure 11). Similar reasoning applies to the TRAPDOR experiment for Do3_7, although the hydrocarbon peaks show up at slightly lower ppm values and also the intensity of the hydrocarbons as well as the Mg–OH group appears to be much lower.

The TRADPOR effect was monitored as a function of the offset of the chlorine transmitter to probe the strength of the quadrupolar parameter of the site that couples to the Mg–OH protons (Figure S14). From 2.25 MHz onward, no detectable dephasing occurs anymore, indicating the TRAPDOR cutoff frequency, ν_C, which equals ν_Q in the case of a spin $S = 3/2$ nucleus.[41,66] From this, the C_Q of the coupled ^{35}Cl can be determined, which is found to be 4.5 MHz. This matches perfectly with the ^{35}Cl C_Q of $MgCl_2$, indicating that the Mg–OH protons have an interaction with bulk or bulklike chlorine atoms. Our TRAPDOR experiments fail to show an interaction between the donor and $MgCl_2$. Due to the short T_2 of the donor resonances, the peaks have already dephased completely at longer echo times and potential TRAPDOR effects cannot be observed.

$^1H-^{25}Mg$ Correlation Experiments. Static ^{25}Mg QCPMG experiments yield better signal with ^1H decoupling. In particular for Do3_7 and Do1_10, significantly more echoes can be acquired using decoupling (Figure S15). The line shape, on the other hand, does not seem to be influenced by the decoupling. Also MQMAS experiments performed better using ^1H decoupling. These are the first, rudimentary, proofs of an interaction between ^{25}Mg and protons in these systems. To further investigate this, we attempted to perform $^1H-^{25}Mg$ CP measurements (see Supporting Information (SI)) initially on samples $MgCl_2$ DCM, Do1_10, and Do3_7. The $^1H-^{25}Mg$ CP spectra of the adducts look very comparable to the bulk,

although the S/N ratio is too low to warrant that there are no additional broader signals present. For $MgCl_2$ DCM, a signal could only be detected after 68 h of experimental time (because proton relaxation times were found to be very long (<1 min)), in which 4096 scans were acquired using 20 ms of contact time (see Figure 12A). The spectral quality is poor. Nevertheless, it is remarkable that this intrinsic proton-free sample is able to give a CP signal that looks quite similar to the direct excitation spectrum.

An $^1H-^{25}Mg$ CP spectrum of Do3_7, acquired in 91.5 h at -40 °C, is shown in Figure 12B. While the line shape of the bulk signal appears slightly broader than the QCPMG echo, the overall line shape agrees very well with the QCPMG echo. Both the CP and QCPMG spectrum show the broad component between -200 and 200 ppm with the same relative intensities (see also Figure S16A). All in all, this correspondence in line shape and long relaxation times discouraged us to continue with CP experiments. However, the similarity between DP and CP spectra requires an explanation. Also, the observation of CP signal for $MgCl_2$ DCM is unexpected due to the low proton content in this sample. Clearly, bulklike sites are in the vicinity of some source of protons. These bulklike sites could either be the layers just below the surface or perhaps the (001)-surfaces. The latter surface sites have quadrupole parameters close to the bulk, yet no donors or –OH groups should coordinate to these (001)-surfaces. The protons that are involved in the CP were further probed using correlation experiments.

Correlation experiments such as $^{25}Mg-\{^1H\}$ ssDFS-REDOR-QCPMG, $^1H-\{^{25}Mg\}$ REDOR, and $^1H-^{25}Mg$ HETCOR experiments have been performed to study the H–Mg interaction(s) (see SI). Similar to the $^{35}Cl-\{^1H\}$ REDOR experiment, the $^{25}Mg-\{^1H\}$ REDOR experiments show clear X–H interactions (Figure S17), while for technical reasons, no interactions could be seen in $^1H-\{^{25}Mg\}$ REDOR and HETCOR experiments (Figures S18 and S19).

For the $^{25}Mg-\{^1H\}$ REDOR experiments, there is quite a difference between the samples, with some showing a pronounced REDOR effect, while for others, the effect is only small. The REDOR fraction, $\Delta S/S_0$, goes up to 17 and 24% for Do1_10 and Do3_7, respectively. For $MgCl_2$ DCM and $MgCl_2-TiCl_4$ adduct, the REDOR effect is only marginal, showcasing a much weaker $^1H-^{25}Mg$ dipolar interaction.

Remarkably, $MgCl_2$ DCM showed a significant effect in the $^{35}Cl-\{^1H\}$ REDOR experiment. Owing to the ssDFS and

QCPMG elements, the ^{25}Mg spectra show both the bulk signal and the surface site for Do1_4, Do3_7, and the TiCl$_4$ adduct. This clearly shows that only REDOR effects are observed for the signal from the bulk phase, and the surface sites are never influenced by the refocusing pulses on the proton channel. Also in ^{35}Cl−{^{1}H} REDOR experiments (vide supra), an X−H interaction (resulting from −OH groups) with the bulk was found. As the surface sites could not be observed in the ^{35}Cl REDOR experiments, we cannot establish if there is an interaction between protons and chlorines at the surface.

Implications. The analysis of ^{25}Mg/^{35}Cl−^{1}H correlations experiments gives some intriguing results. An H−X interaction between Mg−OH protons and the bulk of MgCl$_2$ is detected, while interactions between the donor and the support could not be established. Only in the case of ^{1}H−^{25}Mg CP experiments, there is a correlation between the surface sites and protons, which was not found in the ^{25}Mg−{^{1}H} REDOR experiments.

Most intriguing results have been obtained for sample Do1_10. Both ^{25}Mg and ^{35}Cl show interesting differences compared to the other adducts. The absence of surface sites in ^{25}Mg QCPMG experiments can still be explained by the formation of surface sites with low C_Q (of similar value as the bulk), in agreement with computational results for the suggested model, which was identified based on ^{13}C NMR results. However, the spectrum of Do1_4 is significantly different, which is unexpected since ^{13}C NMR results suggest that both samples have predominantly the same surface structure for the donor, with Do1_4 only having a minor contribution of an additional conformer. The high ^{35}Cl visibility of Do1_10 is not in line with its large surface area, suggesting the formation of surface sites with lower ^{35}Cl quadrupolar coupling parameters that are indeed detected using ^{35}Cl Hahn echoes at high RF power. These findings do not conform to the calculated quadrupolar coupling parameters from the suggested surface structure. All in all, there are some inconsistencies in the results from quadrupolar NMR studies that do not allow us to either confirm or reject the proposed surface model for DMDOMe. One explanation for this might lie in the dynamics at the surface. This is very demanding to accommodate into DFT calculations, but it could have pronounced influence on some spectral aspects.

Considering the other adsorbates, the ^{35}Cl NMR results are in agreement with the large C_Q values for the exposed surface sites (either coordinated or not). However, the unresponsiveness of the ^{35}Cl C_Q to donor adsorption makes it impossible to detect coordinated and bare surface sites independently. The observation of surface sites in ^{25}Mg QCPMG experiments is interesting and confusing at the same time. In particular, the span of these resonances indicates larger quadrupole coupling parameters than what have been calculated. Also, the high relative intensities of these resonances do not conform to the fraction of coordinated surface sites. It could very well be that also magnesium sites in the next shell contribute to the broader signals. Surface deformations can change the local symmetry of these otherwise coordinatively saturated sites, increasing their quadrupolar coupling parameters. Moreover, there may well be many defects in the sample induced by the ball milling.

Despite different approaches, we have not been able to measure interactions between the donor and the support. Although protons have shown interactions, the observed effects did not originate from the donors. Low resolution and short T_2 hamper the further application of proton NMR, and more demanding experiments, involving, for example, ^{13}C, are required. Intrinsically, ^{13}C−^{25}Mg/^{35}Cl correlation experiments sound very appealing; unfortunately, they are not feasible. The main limitation for this is the sensitivity, due to the dilution of the relevant species, low natural abundance of the involved nuclei (^{13}C, ^{25}Mg), and their low gyromagnetic ratio leading to low receptivity. Although costly, a boost in the sensitivity could be obtained by (selective) isotope labeling of ^{13}C and/or ^{25}Mg.

■ CONCLUSIONS

We showed DFT calculations of the ^{25}Mg/^{35}Cl electric field gradient (EFG) tensor and ^{25}Mg/^{35}Cl solid-state NMR spectra for a series of binary adducts between MgCl$_2$ and TiCl$_4$ or MgCl$_2$ and electron donors. These samples have been investigated as model systems to Ziegler−Natta catalysts. In particular, we have been looking into the surface structures formed by different donors to find experimental evidence for suggested models. Correlation experiments clearly show X−H interactions, but they ultimately involved the Mg−OH surface group as source of the proton polarization. The interactions were found to occur between the OH group and bulklike sites.

In general, for magnesium, DFT calculations show pronounced reduction of the quadrupolar interaction (C_Q) for each case, where octahedral coordination is restored at the surface. In some cases, the resulting C_Q becomes almost the same as the bulk value. For chlorine surface sites, on the other hand, the coordination of adsorbates has only a minor effect, which means that chlorine surface sites will continue to give broad lines also after coordination of a donor. This is in line with the visibility of Hahn echoes of the central transition (low ν_{RF}), in which up to 20% of the expected signal intensity is missing. Echo experiments, obtained using high RF fields, indeed show the presence of chlorine sites with low local symmetry, i.e., large quadrupole parameters ($C_Q > 10$ MHz) for the small-particle DiBP adduct (Do3_7).

The DMDOMe adduct behaves quite differently compared to the other adducts. In ^{25}Mg QCPMG and ssDFS-QCPMG experiments, the spectra of all adducts clearly indicate the presence of a second component for most samples, but this is absent in Do1_10. Also, it has a surprisingly high ^{35}Cl visibility given its small particle size. Besides sites with large quadrupole parameters, echo experiments obtained at high RF power show an additional signal with an intermediately large quadrupole parameter ($C_Q \sim 8$ MHz) for this sample. This is not in line with calculated NMR parameters from the suggested model. We should therefore consider a notably different surface structure for Do1_10, in which both ^{25}Mg and ^{35}Cl C_Q are affected by the donor coordination.

We found that it is not feasible to use ^{35}Cl C_Q for the interpretation of specific structural models. In that respect, the ^{25}Mg quadrupolar interaction parameters seem much more promising as they are strongly influenced by donor binding, both experimentally and computationally, and also show significant structural variations. Further research employing solid-state NMR should focus on ^{25}Mg NMR as a very valuable source of structural information.

Identifying specific surface structures by comparing NMR results to DFT calculations proved to be difficult in all cases. This is partly attributed to the existence of many defect structures caused by the ball-milling process used to prepare the samples. The existence of such defect structures both at the surface and in the interior of the MgCl$_2$ particles is obvious from T_1 relaxation studies of the adducts, which display large

difference in relaxivity as a function of particle size/ball-milling time.

EXPERIMENTAL SECTION

Sample Preparation. The preparation of the samples studied in this contribution is described elsewhere.[34] In short, dried $MgCl_2$ and the respective donors were ball-milled for 8 h. The resulting solid was then washed with one or more aliquots of dry heptane and pentane under vigorous stirring at room temperature and finally dried under vacuum at 50 °C overnight.

Computational Details. Quadrupolar parameters were calculated by means of a well-known periodic ab initio software package, namely, the CRYSTAL09 suite,[67] which uses atom-centered (Gaussian) basis sets.

Geometry optimizations and electric field gradient (EFG) calculations were carried out at the B3LYP[68] level of theory, including Grimme's (D2) semiempirical correction[69] for dispersion (with the modification proposed by Civalleri and co-workers[70]), using the TZVP basis set[11] for Mg, Cl, and Ti, and Ahlrichs VTZ plus polarization basis set[71] for the C, H, and O atoms (optimized in a previous work[12]). In the case of $MgCl_2-nH_2O$, the EFG calculations were carried out using the pob-TZVP basis set[72] for Cl atoms. The positions of all atoms were fully relaxed along with the cell parameters. With reference to the CRYSTAL09 user manual,[67] in the evaluation of the Coulomb and Hartree–Fock exchange series, the five threshold parameters determining the level of accuracy were set at 7, 7, 7, 7, and 18 values. The threshold on the self-consistent field energy was set to 10^{-8} Ha for the geometry optimizations. The reciprocal space was sampled according to a regular sublattice with shrinking factor equal to 6.

In the case of the DiBP adducts and the high-coverage model of the DMDOMe adduct, we adopt the cluster approach described elsewhere.[34,73] The optimized cluster structures are reproduced in the SI. The EFG calculations were carried out at the TPSSTPSS[74] level using the 6-31+G(2d,p) basis set[75] for Mg and Cl, and the IGLO-II basis set[76] for H, C, and O atoms.

NMR. ^{25}Mg and ^{35}Cl spectra were recorded at room temperature on a Varian VNMRS 850 MHz spectrometer (20 T, 52.0 MHz for ^{25}Mg, 83.25 MHz for ^{35}Cl) using a triple-resonance 4.0 mm Varian T3 MAS probe at 15.625 kHz MAS. ^{25}Mg and ^{35}Cl spectra have been obtained using a Hahn echo with short echo times: 1 rotor period (64 μs) or 16 μs (static). Recycle delays were long enough (3–5 times T_1) to ensure quantitative measurements. Shifts were referenced to solid NaCl (δ_{iso} = −45.37 ppm with respect to infinitely dilute solution of NaCl(aq) (δ_{iso} = 0.0 ppm)) or a saturated solution of $MgCl_2$(aq) (set to 0.0 ppm).

We used the sideband-selective double-frequency sweep (ssDFS) pulse scheme[61] to transfer population from the satellites into the central transition to increase the signal. A theoretical maximum enhancement of 2I can be obtained using this technique. We also used the QCPMG detection scheme.[77−79] A series of echo pulses is applied with signal detection between the echoes. This leads to the so-called spikelet spectrum, in which the regular Hahn-echo signal is split into a manifold of sharp lines (spikelets), which resembles the envelope of the echo spectrum. Since the intensity of the echo is distributed over a few spikelets, the signal-to-noise ratio increases significantly. As shown before,[80] we combined ssDFS and QCPMG to get maximum enhancement.

ASSOCIATED CONTENT

Supporting Information

The Supporting Information is available free of charge on the ACS Publications website at DOI: 10.1021/acs.jpcc.8b05123.

Additional solid-state NMR spectra and optimized structures of cluster models (PDF)

AUTHOR INFORMATION

Corresponding Author
*E-mail: a.kentgens@nmr.ru.nl.

ORCID
E. S. Merijn Blaakmeer: 0000-0001-5108-5655
Giuseppe Antinucci: 0000-0003-1258-6363
Arno P. M. Kentgens: 0000-0001-5893-4488

Notes
The authors declare no competing financial interest.

REFERENCES

(1) Moore, E. P. J., Ed. *Polypropylene Handbook: Polymerization, Characterization, Properties, Processing, Applications*; Hanser Publishers: Munich, Germany, 1996.

(2) Cecchin, G.; Morini, G.; Piemontesi, F. *Kirk-Othmer Encyclopedia of Chemical Technology*; John Wiley & Sons, Inc.: New York, 2000.

(3) Seth, M.; Margl, P. M.; Ziegler, T. A Density Functional Embedded Cluster Study of Proposed Active Sites in Heterogeneous Ziegler-Natta Catalysts. *Macromolecules* 2002, 35, 7815−7829.

(4) Stukalov, D. V.; Zakharov, V. A.; Potapov, A. G.; Bukatov, G. D. Supported Ziegler-Natta Catalysts for Propylene Polymerization. Study of Surface Species Formed at Interaction of Electron Donors and $TiCl_4$ with Activated $MgCl_2$. *J. Catal.* 2009, 266, 39−49.

(5) Stukalov, D. V.; Zakharov, V. A.; Zilberberg, I. L. Adsorption Species of Ethyl Benzoate in $MgCl_2$-Supported Ziegler-Natta Catalysts. A Density Functional Theory Study. *J. Phys. Chem. C* 2010, 114, 429−435.

(6) Credendino, R.; Busico, V.; Causà, M.; Barone, V.; Budzelaar, P. H. M.; Zicovich-Wilson, C. Periodic DFT Modeling of Bulk and Surface Properties of $MgCl_2$. *Phys. Chem. Chem. Phys.* 2009, 11, 6525−6532.

(7) Credendino, R.; Pater, J. T. M.; Correa, A.; Morini, G.; Cavallo, L. Thermodynamics of Formation of Uncovered and Dimethyl Ether-Covered $MgCl_2$ Crystallites. Consequences in the Structure of Ziegler-Natta Heterogeneous Catalysts. *J. Phys. Chem. C* 2011, 115, 13322−13328.

(8) Credendino, R.; Liguori, D.; Morini, G.; Cavallo, L. Investigating Phthalate and 1,3-Diether Coverage and Dynamics on the (104) and (110) Surfaces of $MgCl_2$-Supported Ziegler-Natta Catalysts. *J. Phys. Chem. C* 2014, 118, 8050−8058.

(9) Credendino, R.; Liguori, D.; Fan, Z.; Morini, G.; Cavallo, L. Toward a Unified Model Explaining Heterogeneous Ziegler-Natta Catalysis. *ACS Catal.* 2015, 5, 5431−5435.

(10) Brambilla, L.; Zerbi, G.; Piemontesi, F.; Nascetti, S.; Morini, G. Structure of Donor Molecule 9,9-Bis(Methoxymethyl)-Fluorene in Ziegler-Natta Catalyst by Infrared Spectroscopy and Quantum Chemical Calculation. *J. Phys. Chem. C* 2010, 114, 11475−11484.

(11) D'Amore, M.; Credendino, R.; Budzelaar, P. H.; Causà, M.; Busico, V. A Periodic Hybrid DFT Approach (Including Dispersion) to MgCl$_2$-Supported Ziegler-Natta catalysts - 1: TiCl$_4$ Adsorption on MgCl$_2$ Crystal Surfaces. *J. Catal.* 2012, 286, 103−110.

(12) Capone, F.; Rongo, L.; D'Amore, M.; Budzelaar, P. H. M.; Busico, V. Periodic Hybrid DFT Approach (Including Dispersion) to MgCl$_2$-Supported Ziegler-Natta Catalysts. 2. Model Electron Donor Adsorption on MgCl$_2$ Crystal Surfaces. *J. Phys. Chem. C* 2013, 117, 24345−24353.

(13) Correa, A.; Credendino, R.; Pater, J. T. M.; Morini, G.; Cavallo, L. Theoretical Investigation of Active Sites at the Corners of MgCl$_2$-Crystallites in Supported Ziegler-Natta Catalysts. *Macromolecules* 2012, 45, 3695−3701.

(14) Bazhenov, A. S.; Denifl, P.; Leinonen, T.; Pakkanen, A.; Linnolahti, M.; Pakkanen, T. A. Modeling Coadsorption of Titanium Tetrachloride and Bidentate Electron Donors on Magnesium Dichloride Support Surfaces. *J. Phys. Chem. C* 2014, 118, 27878−27883.

(15) Bazhenov, A.; Linnolahti, M.; Pakkanen, T. A.; Denifl, P.; Leinonen, T. Modeling the Stabilization of Surface Defects by Donors in Ziegler-Natta Catalyst Support. *J. Phys. Chem. C* 2014, 118, 4791−4796.

(16) Kuklin, M. S.; Bazhenov, A. S.; Denifl, P.; Leinonen, T.; Linnolahti, M.; Pakkanen, T. A. Stabilization of Magnesium Dichloride Surface Defects by Mono- and Bidentate Donors. *Surf. Sci.* 2015, 635, 5−10.

(17) Correa, A.; Piemontesi, F.; Morini, G.; Cavallo, L. Key Elements in the Structure and Function Relationship of the MgCl$_2$/TiCl$_4$/Lewis Base Ziegler-Natta Catalytic System. *Macromolecules* 2007, 40, 9181−9189.

(18) Shetty, S. Synergistic, Reconstruction and Bonding Effects during the Adsorption of Internal Electron Donors and TiCl$_4$ on MgCl$_2$-Surface: A Periodic-DFT Investigation. *Surf. Sci.* 2016, 653, 55−65.

(19) Kumawat, J.; Kumar Gupta, V.; Vanka, K. The Nature of the Active Site in Ziegler-Natta Olefin Polymerization Catalysis Systems - A Computational Investigation. *Eur. J. Inorg. Chem.* 2014, 2014, 5063−5076.

(20) Kumawat, J.; Gupta, V. K.; Vanka, K. Effect of Donors on the Activation Mechanism in Ziegler-Natta Catalysis: A Computational Study. *ChemCatChem* 2016, 8, 1809−1818.

(21) Linnolahti, M.; Pakkanen, T. A.; Bazhenov, A. S.; Denifl, P.; Leinonen, T.; Pakkanen, A. Alkylation of Titanium Tetrachloride on Magnesium Dichloride in the Presence of Lewis Bases. *J. Catal.* 2017, 353, 89−98.

(22) D'Amore, M.; Thushara, K. S.; Piovano, A.; Causà, M.; Bordiga, S.; Groppo, E. Surface Investigation and Morphological Analysis of Structurally Disordered MgCl$_2$ and MgCl$_2$/TiCl$_4$ Ziegler-Natta Catalysts. *ACS Catal.* 2016, 6, 5786−5796.

(23) Thushara, K. S.; D'Amore, M.; Piovano, A.; Bordiga, S.; Groppo, E. The Influence of Alcohols in Driving the Morphology of Magnesium Chloride Nanocrystals. *ChemCatChem* 2017, 9, 1782−1787.

(24) Tkachenko, O. P.; Kucherov, A. V.; Kustov, L. M.; Virkkunen, V.; Leinonen, T.; Denifl, P. A Study of Ziegler-Natta Propylene Polymerization Catalysts by Spectroscopic Methods. *Materials* 2017, 10, 496−512.

(25) Gnanakumar, E. S.; Gowda, R. R.; Kunjir, S.; Ajithkumar, T. G.; Rajamohanan, P. R.; Chakraborty, D.; Gopinath, C. S. MgCl$_2$·6CH$_3$OH: A Simple Molecular Adduct and Its Influence As a Porous Support for Olefin Polymerization. *ACS Catal.* 2013, 3, 303−311.

(26) Gnanakumar, E. S.; Rao Chokkapu, E.; Kunjir, S.; Ajithkumar, T. G.; Rajamohanan, P. R.; Chakraborty, D.; Gopinath, C. S. 9-Fluorenemethanol: An Internal Electron Donor to Fine Tune Olefin Polymerization Activity. *Dalton Trans.* 2014, 43, 9143.

(27) Sobota, P.; Utko, J.; Lis, T.; John, L.; Petrus, R.; Drąg-Jarząbek, A. Unexpected Reactions between Ziegler-Natta Catalyst Components and Structural Characterization of Resulting Intermediates. *Inorg. Chem.* 2016, 55, 4636−4642.

(28) Nissinen, V. H.; Linnolahti, M.; Pakkanen, T. T. Methoxymagnesium Chloride: Structure and Interaction with Electron Donors: Experimental and Computational Study. *J. Phys. Chem. C* 2016, 120, 21505−21511.

(29) Nissinen, V. H.; Koshevoy, I. O.; Pakkanen, T. T. Crystalline Magnesium Chloride-Electron Donor Complexes: New Support Materials for Ziegler-Natta Catalysts. *Dalton Trans.* 2017, 46, 4452−4460.

(30) Vittoria, A.; Meppelder, A.; Friederichs, N.; Busico, V.; Cipullo, R. Demystifying Ziegler-Natta Catalysts: The Origin of Stereoselectivity. *ACS Catal.* 2017, 7, 4509−4518.

(31) Tijssen, K. C. H.; Blaakmeer, E. S.; Kentgens, A. P. M. Solid-State NMR studies of Ziegler-Natta and Metallocene Catalysts. *Solid State Nucl. Magn. Reson.* 2015, 68−69, 37−56.

(32) Grau, E.; Lesage, A.; Norsic, S.; Copéret, C.; Monteil, V.; Sautet, P. Tetrahydrofuran in TiCl$_4$/THF/MgCl$_2$: A Non-Innocent Ligand for Supported Ziegler-Natta Polymerization Catalysts. *ACS Catal.* 2013, 3, 52−56.

(33) D'Anna, V.; Norsic, S.; Gajan, D.; Sanders, K.; Pell, A. J.; Lesage, A.; Monteil, V.; Copéret, C.; Pintacuda, G.; Sautet, P. Structural Characterization of the EtOH-TiCl$_4$-MgCl$_2$ Ziegler-Natta Precatalyst. *J. Phys. Chem. C* 2016, 120, 18075−18087.

(34) Blaakmeer, E. S. M.; Antinucci, G.; Correa, A.; Busico, V.; van Eck, E. R. H.; Kentgens, A. P. M. Structural Characterization of Electron Donors in Ziegler-Natta Catalysts. *J. Phys. Chem. C* 2018, 122, 5525−5536.

(35) Copéret, C.; Comas-Vives, A.; Conley, M. P.; Estes, D. P.; Fedorov, A.; Mougel, V.; Nagae, H.; Núñez-Zarur, F.; Zhizhko, P. A. Surface Organometallic and Coordination Chemistry toward Single-Site Heterogeneous Catalysts: Strategies, Methods, Structures, and Activities. *Chem. Rev.* 2016, 116, 323−421.

(36) Lapina, O. B. Modern ssNMR for Heterogeneous Catalysis. *Catal. Today* 2017, 285, 179−193.

(37) Gullion, T.; Schaefer, J. Rotational-Echo Double Resonance NMR. *J. Magn. Reson. (1969)* 1989, 81, 196−200.

(38) Gullion, T.; Schaefer, J. Elimination of Resonance Offset Effects in Rotational-Echo, Double-Resonance NMR. *J. Magn. Reson. (1969)* 1991, 92, 439−442.

(39) van Eck, E. R. H.; Janssen, R.; Maas, W. E. J. R.; Veeman, W. S. A Novel Application of Nuclear Spin-Echo Double-Resonance to Aluminophosphates and Aluminosilicates. *Chem. Phys. Lett.* 1990, 174, 428−432.

(40) Grey, C. P.; Veeman, W. S.; Vega, A. J. Rotational Echo ^{14}N/^{13}C/^{1}H Triple Resonance Solid-State Nuclear Magnetic Resonance: A Probe of ^{13}C-^{14}N Internuclear Distances. *J. Chem. Phys.* 1993, 98, 7711−7724.

(41) Grey, C. P.; Vega, A. J. Determination of the Quadrupole Coupling Constant of the Invisible Aluminum Spins in Zeolite HY with ^{1}H/^{27}Al TRAPDOR NMR. *J. Am. Chem. Soc.* 1995, 117, 8232−8242.

(42) Blaakmeer, E. S.; Antinucci, G.; Busico, V.; van Eck, E. R. H.; Kentgens, A. P. M. Solid-State NMR Investigations of MgCl$_2$ Catalyst Support. *J. Phys. Chem. C* 2016, 120, 6063−6074.

(43) Pasquini, N. *Polypropylene Handbook*, 2nd ed.; Hanser Publishers: Munich, 2005.

(44) Kaminsky, W. *Polyolefins: 50 Years after Ziegler and Natta I Polyethylene and Polypropylene*, 1st ed.; Advances in Polymer Science; Springer-Verlag: Berlin, 2013; Vol. 257.

(45) Kentgens, A. P. M. In *Encyclopedia of Magnetic Resonance*; Harris, R. K., Wasylishen, R., Eds.; John Wiley: Chichester, 2011.

(46) Le Caër, G.; Bureau, B.; Massiot, D. An Extension of the Czjzek Model for the Distributions of Electric Field Gradients in Disordered Solids and an Application to NMR Spectra of ^{71}Ga in Chalcogenide Glasses. *J. Phys.: Condens. Matter* 2010, 22, No. 065402.

(47) Knijn, P. J.; van Bentum, P. J. M.; van Eck, E. R. H.; Fang, C.; Grimminck, D. L. A. G.; de Groot, R. A.; Havenith, R. W. A.; Marsman, M.; Meerts, W. L.; de Wijs, G. A.; et al. A Solid-State NMR and DFT study of Compositional Modulations in Al$_x$Ga$_{1-x}$As. *Phys. Chem. Chem. Phys.* 2010, 12, 11517.

(48) Czjzek, G.; Fink, J.; Götz, F.; Schmidt, H.; Coey, J. M. D.; Rebouillat, J.-P.; Liénard, A. Atomic Coordination and the Distribution of Electric Field Gradients in Amorphous Solids. *Phys. Rev. B* **1981**, *23*, 2513−2530.

(49) d'Espinose de Lacaillerie, J.-B.; Fretigny, C.; Massiot, D. MAS NMR spectra of quadrupolar nuclei in disordered solids: The Czjzek model. *J. Magn. Reson.* **2008**, *192*, 244−251.

(50) Bureau, B.; Guérault, H.; Silly, G.; Buzaré, J. Y.; Grenèche, J. M. NMR Investigation of Mechanically Milled Nanostructured GaF₃ Powders. *J. Phys.: Condens. Matter* **1999**, *11*, L423.

(51) Scholz, G.; Stösser, R.; Klein, J.; Silly, G.; Buzaré, J. Y.; Laligant, Y.; Ziemer, B. Local Structural Orders in Nanostructured Al₂O₃ Prepared by High-Energy Ball Milling. *J. Phys.: Condens. Matter* **2002**, *14*, 2101.

(52) Grimminck, D. L.; Polman, B. J.; Kentgens, A. P.; Leo Meerts, W. EASY-GOING Deconvolution: Combining Accurate Simulation and Evolutionary Algorithms for Fast Deconvolution of Solid-State Quadrupolar NMR Spectra. *J. Magn. Reson.* **2011**, *211*, 114−120.

(53) Andrew, E.; Tunstall, D. Spin-Lattice Relaxation in Imperfect Cubic Crystals and in Non-cubic Crystals. *Proc. Phys. Soc.* **1961**, *78*, 1−11.

(54) Haase, J.; Park, K. D.; Guo, K.; Timken, H. K. C.; Oldfield, E. Nuclear Magnetic Resonance Spectroscopic Study of Spin-Lattice Relaxation of Quadrupolar Nuclei in Zeolites. *J. Phys. Chem.* **1991**, *95*, 6996−7002.

(55) Freude, D.; Haase, J. In *NMR Basic Principles and Progress*; Pfeifer, H., Ed.; Springer-Verlag: Berlin, Heidelberg, 1993; Vol. *29*, pp 3−90.

(56) Breuza, E.; Antinucci, G.; Ehm, C.; Buzelaar, P. H. M.; Buscio, V.; Correa, A. MgCl₂-Supported Ziegler-Natta Catalysts: A DFT-D Flexible-Cluster Approach. TiCl₄ and Probe Donor Adducts. *Int. J. Quantum Chem.*, submitted for publication, 2018.

(57) Johnston, K. E.; O'Keefe, C. A.; Gauvin, R. M.; Trébosc, J.; Delevoye, L.; Amoureux, J.-P.; Popoff, N.; Taoufik, M.; Oudatchin, K.; Schurko, R. W. A Study of Transition-Metal Organometallic Complexes Combining ³⁵Cl Solid-State NMR Spectroscopy and ³⁵Cl NQR Spectroscopy and First-Principles DFT Calculations. *Chem. − Eur. J.* **2013**, *19*, 12396−12414.

(58) Blaakmeer, E. S. M.; Franssen, W. M. J.; Kentgens, A. P. M. Quadrupolar Nutation NMR to Discriminate between Central and Satellite Transitions: Spectral Assignment for a Ziegler-Natta Catalyst. *J. Magn. Reson.* **2017**, *281*, 199−208.

(59) Frydman, L.; Harwood, J. S. Isotropic Spectra of Half-Integer Quadrupolar Spins from Bidimensional Magic-Angle Spinning NMR. *J. Am. Chem. Soc.* **1995**, *117*, 5367−5368.

(60) Medek, A.; Harwood, J. S.; Frydman, L. Multiple-Quantum Magic-Angle Spinning NMR: A New Method for the Study of Quadrupolar Nuclei in Solids. *J. Am. Chem. Soc.* **1995**, *117*, 12779−12787.

(61) Goswami, M.; van Bentum, P.; Kentgens, A. Sensitivity Enhancement in MAS NMR of Half-Integer Quadrupolar Nuclei using Sideband Selective Double-Frequency Sweeps. *Can. J. Chem.* **2011**, *89*, 1130−1137.

(62) Harris, R. K.; Nesbitt, G. J. Cross Polarization for Quadrupolar Nuclei - Proton to Sodium-23. *J. Magn. Reson. (1969)* **1988**, *78*, 245−256.

(63) Phillips, B. L.; Burnley, P. C.; Worminghaus, K.; Navrotsky, A. ²⁹Si and ¹H NMR Spectroscopy of High-Pressure Hydrous Magnesium Silicates. *Phys. Chem. Miner.* **1997**, *24*, 179−190.

(64) Xue, X.; Kanzaki, M. High-Pressure δ-Al(OH)₃ and δ-AlOOH Phases and Isostructural Hydroxides/Oxyhydroxides: New Structural Insights from High-Resolution H-1 and Al-27 NMR. *J. Phys. Chem. B* **2007**, *111*, 13156−13166.

(65) Xue, X.; Kanzaki, M. Proton Distributions and Hydrogen Bonding in Crystalline and Glassy Hydrous Silicates and Related Inorganic Materials: Insights from High-Resolution Solid-State Nuclear Magnetic Resonance Spectroscopy. *J. Am. Ceram. Soc.* **2009**, *92*, 2803−2830.

(66) Zeng, Q.; Nekvasil, H.; Grey, C. P. Proton Environments in Hydrous Aluminosilicate Glasses: A ¹H MAS, ¹H/²⁷Al, and ¹H/²³Na TRAPDOR NMR Study. *J. Phys. Chem. B* **1999**, *103*, 7406−7415.

(67) Dovesi, R.; Saunders, V. R.; Orlando, R.; Zicovich-Wilson, C. M.; Pascale, F.; Civalleri, B.; Doll, K.; Bush, I. J.; D'Arco, P.; Lunell, M. Crystal 2009 User Manual, 2009.

(68) Becke, A. D. Density-Functional Thermochemistry. III. The Role of Exact Exchange. *J. Chem. Phys.* **1993**, *98*, 5648−5652.

(69) Grimme, S. Semiempirical GGA-Type Density Functional Constructed with a Long-Range Dispersion Correction. *J. Comput. Chem.* **2006**, *27*, 1787−1799.

(70) Civalleri, B.; Zicovich-Wilson, C. M.; Valenzano, L.; Ugliengo, P. B3LYP Augmented with an Empirical Dispersion Term (B3LYP-D*) as Applied to Molecular Crystals. *CrystEngComm* **2008**, *10*, 405−410.

(71) Schäfer, A.; Horn, H.; Ahlrichs, R. Fully Optimized Contracted Gaussian Basis Sets for Atoms Li to Kr. *J. Chem. Phys.* **1992**, *97*, 2571−2577.

(72) Peintinger, M. F.; Oliveira, D. V.; Bredow, T. Consistent Gaussian Basis Sets of Triple-Zeta Valence with Polarization Quality for Solid-State Calculations. *J. Comput. Chem.* **2013**, *34*, 451−459.

(73) Breuza, E.; Antinucci, G.; Buzelaar, P. H. M.; Buscio, V.; Correa, A.; Ehm, C. MgCl₂-Supported Ziegler-Natta Catalysts: A DFT-D 'Flexible-Cluster' Approach. Internal Donor Adducts. *J. Phys. Chem. C* **2018**, *122*, 9046−9053.

(74) Tao, J.; Perdew, J. P.; Staroverov, V. N.; Scuseria, G. E. Climbing the Density Functional Ladder: Nonempirical Meta-Generalized Gradient Approximation Designed for Molecules and Solids. *Phys. Rev. Lett.* **2003**, *91*, No. 146401.

(75) Rassolov, V. A.; Ratner, M. A.; Pople, J. A.; Redfern, P. C.; Curtiss, L. A. 6-31G*Basis Set for Third-Row Atoms. *J. Comput. Chem.* **2001**, *22*, 976−984.

(76) Kutzelnigg, W.; Fleischer, U.; Schindler, M. The IGLO-Method: Ab-initio Calculation and Interpretation of NMR Chemical Shifts and Magnetic Susceptibilities. *NMR: Basic Princ. Prog.* **1990**, 165−262.

(77) Larsen, F. H.; Jakobsen, H. J.; Ellis, P. D.; Nielsen, N. C. Sensitivity-Enhanced Quadrupolar-Echo NMR of Half-Integer Quadrupolar Nuclei. Magnitudes and Relative Orientation of Chemical Shielding and Quadrupolar Coupling Tensors. *J. Phys. Chem. A* **1997**, *101*, 8597−8606.

(78) Larsen, F. H.; Jakobsen, H. J.; Ellis, P. D.; Nielsen, N. C. QCPMG-MAS NMR of Half-Integer Quadrupolar Nuclei. *J. Magn. Reson.* **1998**, *131*, 144−147.

(79) Larsen, F. H.; Skibsted, J.; Jakobsen, H. J.; Nielsen, N. C. Solid-State QCPMG NMR of Low-γ Quadrupolar Metal Nuclei in Natural Abundance. *J. Am. Chem. Soc.* **2000**, *122*, 7080−7086.

(80) Blaakmeer, E. S.; Rosciano, F.; van Eck, E. R. H. Lithium Doping of MgAl₂O₄ and ZnAl₂O₄ Investigated by High-Resolution Solid State NMR. *J. Phys. Chem. C* **2015**, *119*, 7565−7577.